MODELING STEREOSELECTIVE REACTIONS IN SOLUTION

by

Aslı Yıldırım

B.S., Chemistry, Boğaziçi University, 2010

Submitted to the Institute for Graduate Studies in
Science and Engineering in partial fulfillment of
the requirements for the degree of
Master of Science

Graduate Program in Chemistry

Boğaziçi University

2012

MODELING STEREOSELECTIVE REACTIONS IN SOLUTION

APPROVED BY:

Prof. Viktorya Aviyente …….
(Thesis Supervisor)

Prof. İlknur Doğan …….

Assist. Prof. F. Aylin Sungur …….

DATE OF APPROVAL: 05.06.2012

To my family

ACKNOWLEDGEMENTS

I would like to express my sincere gratitude to my thesis advisor Prof. Viktorya Aviyente for her courage, endless patience and assistance throughout my studies. It was a great opportunity to study in her group and improve myself thanks to her useful comments and excellent scientific guidance.

I wish to appreciate to the members of my committee: Prof. İlknur Doğan (Boğaziçi University) and Assist. Prof. F. Aylin Sungur (Istanbul Technical University) for giving their valuable time and advices.

I would like to extend my thanks to Dr. Şaron Çatak for her availability, support and extensive scientific guidance during my stay in Ghent University.

I would like to thank to all the members of Computational Chemistry Group, Özlem Karahan, Tuğba Furuncuoğlu, Gülşah Çifci, Sesil Agopcan, Berna Doğan, İlke Uğur, Burcu Dedeoğlu and Esra Bozkurt for their enjoyable company and valuable contributions to my studies and especially to Hasan H. İnce for his additional support and friendship. I would also like to thank all my friends and all the members of the Chemistry Department who were exactly like a family for me during these years.

Finally, my deepest thanks go to my mother and father, Bahar Demirel and Müfit Yıldırım, my brother, Arca Yıldırım and my friends who are also a part of my family, Özlem Atalay, Sebla Onbulak and Ulaş Uygun for their continuous support and endless love throughout my life.

ABSTRACT

MODELING STEREOSELECTIVE REACTIONS IN SOLUTION

In this study, ring-chain-ring tautomerization and asymmetric desymmetrization reactions are investigated by taking the solvent effect into account. In the first part, ring-chain-ring tautomerization mechanism is investigated by taking the effect of solvation into account in order to explain the enantiomeric interconversion of heterocyclic 2-oxazolidinone derivatives which are isolated as single enantiomers and have potential to be used as axially chiral catalysts. Density functional calculations reveal that there are two possible pathways with two different intermediary species which are amido and imino intermediates. This part of the study sheds light on the mechanistic details of both possible pathways to be able to understand and predict the ring-chain-ring tautomerization mechanism of similar heterocyclic systems. In the second part, the asymmetric desymmetrization mechanism is subjected to a computational analysis in an effort to investigate the alcoholysis of cyclic *meso* anhydrides in the presence of cinchona alkaloids. In the first step of this part of the study, the conformational analysis of cinchona alkaloids is carried out since the conformation plays a crucial role in enantioselectivity. Then, the mechanism of methanolysis of cyclic *meso* anhydrides catalyzed by cinchona alkaloids is considered by studying both stepwise and concerted pathways.

ÖZET

STEREOSEÇİCİ TEPKİMELERİN ÇÖZÜCÜ İÇİNDE MODELLENMESİ

Bu çalışmada, halka-zincir-halka tautomerizasyonu ve asimetrik desimetrizasyon tepkimeleri çözücünün etkisi göz önünde bulundurularak incelenmiştir. Birinci kısımda, 2-oxazolidinon türevlerinin enantiyomerik ara-çevirimlerini açıklayabilmek için halka-zincir-halka tautomerizasyon mekanizması incelenmiştir. 2-oxazolidinon türevleri tek enantiyomer olarak izole edilebilirler ve aksiyal kiral katalist olarak kullanılabilirler. Yoğunluk Fonksiyonu Teorisi (DFT) ile yapılan hesaplamalar, bu mekanizma için ayrı ara ürünlere sahip olan iki olası yol olduğunu göstermiştir. Bu ayrı iki ürün, amido ara-ürünü ve imino ara-ürünü olarak adlandırılmıştır. Çalışmanın bu kısmı, benzer heterosiklik sistemlerin halka-zincir-halka tautomerizasyon mekanizmalarını anlayabilmek ve ön görülerde bulunmak için her iki yolun mekanizmasına ait ayrıntılarına ışık tutar. İkinci kısımda, siklik *mezo* anhidritlerin kınakına alkaloidlerinin varlığında alkoliz mekanizmasının incelenmesi amacıyla asimetrik desimetrizasyon mekanizması hesapsal analize tabi tutulmuştur. Çalışmanın bu kısmının ilk basamağında kınakına alkaloidlerinin konformasyonel analizi gerçekleştirilmiştir; bir sonraki adımda ise siklik *mezo* anhidritlerin kınakına alkaloidlerinin varlığında metanoliz mekanizması hem aşamalı yol hem de tek adımlı yollar dikkate alınarak incelenmiştir.

TABLE OF CONTENTS

LIST OF FIGURES

LIST OF TABLES

LIST OF ACRONYMS/ABBREVIATIONS

$G^{‡}$	Gibbs free energy of activation
B3LYP	Becke-3-parameter Lee-Yang-Parr functional
BMK	Boese-Martin for Kinetics
DFT	Density functional theory
M06-2X	Empirical exchange-correlation functionals
MP2	Møller–Plesset perturbation theory at second order
MPWB1K	Modified Perdew-Wang-Becke 1 Parameter Method for Kinetics
SCS-MP2	Spin-component scaled second-order Møller–Plesset perturbation theory

1. INTRODUCTION

1.1. Ring-Chain-Ring Tautomerization

Ring-chain-ring tautomerization is a process that involves a proton shift assisted ring-opening followed by a ring-closure, and is a significant step in the organic synthesis of five- and six-membered 1,3-heterocycles containing oxygen, nitrogen, or sulfur atoms [1]. In the past decade, the ring-chain tautomeric equilibria has been studied for 1,3-X, *N*-heterocyclic systems (X = S, O) with great interest [2] and has also attracted attention in physical and medicinal chemistry [3].

Recent studies have shown that ring-chain-ring tautomerization is a key pathway for the synthesis of various important compounds. Thiazolidinyloxazolidines and spirothiazolidines, which are analogues of bisoxazolidines notably used as chiral catalysts [4], anticancer [5], and neuroprotective agents [6], have been obtained from the ring-chain tautomerization of mercaptomethyl bisoxazolidine [7]. Furthermore, this process has also been observed in the conversion of bicyclo[4.2.0]octane derivatives to trisubstituted enamines [8].

Two recent studies proved the existence of ring-chain tautomerization in simplified analogues of isoniazid–NAD(P) adducts, which are known for their prominent activity against Mycobacterium tuberculosis [9], and in 2-ferrocenyl-2,4-dihydro-1*H*-3,1-benzoxazines [10].

The ring-chain tautomerization process has been shown to occur in heterocyclic compounds, such as a novel 1,3-imidazolidine containing a vinyloxy group [2a], as well as pyrazolidine, pyridazine and oxazolidine derivatives, which are of particular interest in this study [11, 12].

Compounds comprising the oxazolidine ring, which are also the subject of the present study, have been introduced as drugs for the treatment of insuline resistance, hyperglycemia and some lipid disorders [13-15]. The chemical importance of these

compounds is not limited to medicinal chemistry, oxazolidine derivatives have also been used as directing groups in asymmetric synthesis [16, 17].

In this study, the mechanism of ring-chain-ring tautomerization and the prominent effect of the solvent environment have been computationally investigated, in an effort to explain the enantiomeric interconversion observed in 2-oxazolidinone derivatives – heterocyclic analogues of biphenyl atropisomers– that were isolated as single stable enantiomers and have the potential to be used as axially chiral catalysts. This study sheds light on the identity of the intermediary species involved in the ring-chain-ring tautomerization process as well as the catalytic effect of polar protic solvents. These mechanistic details will prove very useful in predicting and understanding ring-chain tautomeric equilibria in similar heterocyclic systems and will further enable experimentalists to devise the proper experimental conditions where axially chiral catalysts remain stable as single enantiomers.

1.2. Asymmetric Desymmetrization of *Meso* Anhydrides

Asymmetric desymmetrization (AD) of *meso* anydrides which yield chiral products has attracted considerable attention in asymmetric synthesis, because formation of multiple stereogenic centers can be achieved in one symmetry-breaking operation [18-20] and *meso* anhydrides are easily accessible, either from commercial suppliers or by means of chemical transformations such as Diels-Alder reactions of maleic anhydrides. The optically active products of desymmetrization of cyclic *meso* anhydrides are valuable building blocks because they can be used in the synthesis of natural products or biologically active substances [21, 22]. There are numerous ways for diastereoselective and enantioselective anhydride openings with several nucleophiles and chiral catalysts yielding optically active products (Figure 1.1).

The enantioselective asymmetric desymmetrization (AD) of *meso* compounds can be performed by either enzymatic [23] or nonenzymatic methods such as chiral reagents [20]. Desymmetrization of symmetrically substituted diesters or anhydrides with the help of enzymes or chiral reagents gives dicarboxylic acid monoesters that can be used in several synthetic applications (Figure 1.2). However, most of the time only one

enantiomer of the product can be obtained directly when the process is performed enzymatically which can be considered as a disadvantage of the enzymatic method. On the contrary, anhydride openings with chiral nucleophiles are not limited with this restriction, often both enantiomers of the chiral reagent are available.

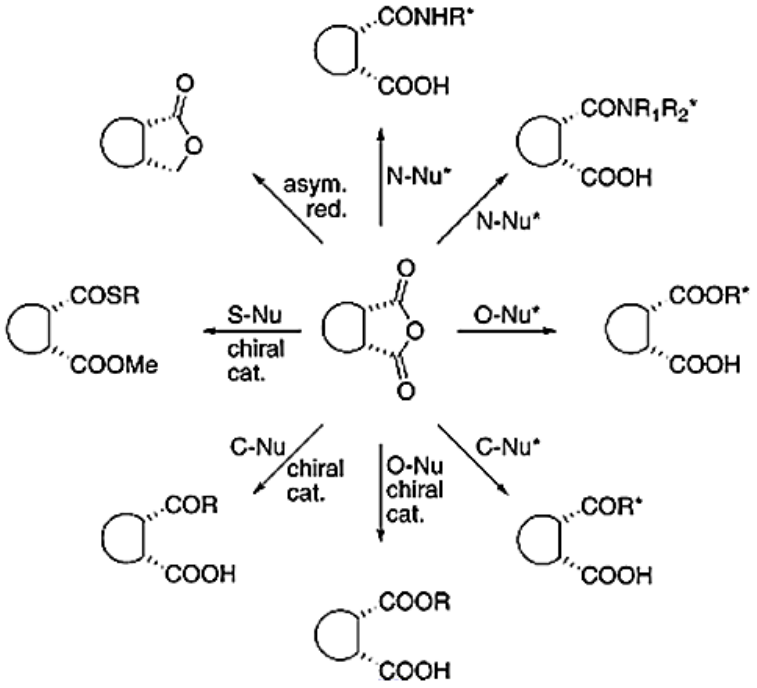

Figure 1.1. Diastereoselective and enantioselective anhydride openings [24].

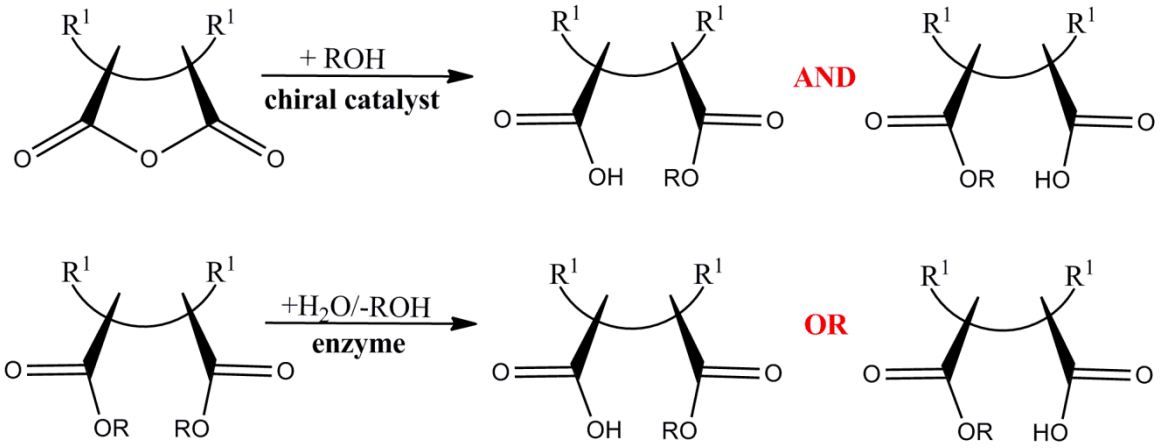

Figure 1.2. General scheme of anhydride desymmetrization with enzymatic and nonenzymatic methods.

If the chiral catalyst to be used in asymmetric desymmetrization of *meso* anhydrides fulfills all the criteria listed below, then the overall utility of the catalyst is ensured:

(i) The variety of reactions that the catalyst can promote
(ii) The availability of both enantiomeric antipodes of the catalyst at a reasonable price
(iii) The stability of the catalyst.

Cinchona alkaloids fulfill all of these criteria making them one of the most powerful catalysts to date. Cinchona alkaloid derived catalysts are central to many catalytic asymmetric reactions today, one of which is the asymmetric desymmetrization (AD) of *meso* cyclic anhydrides. However, the understanding of the principles of the stereoselective anhydride opening lacks a solid basis even though synthetically much progress has been achieved. In this study, the asymmetric desymmetrization of *meso* anhydrides in the presence of cinchona alkaloids will be investigated in order to clarify the mechanism of this reaction.

2. RING-CHAIN-RING TAUTOMERIZATION OF 2-OXAZOLIDINONE DERIVATIVES IN SOLUTION

2.1. Introduction

N-(*o*-aryl)-5,5-dimethyl-2,4-oxazolidinedione derivatives 1, *N*-(*o*-aryl)-rhodanines (X=S) and oxazolidine-2-thiones (X=O) 2 (Figure 2.1) are heterocyclic compounds that have a chiral axis enabling the formation of thermally interconvertible enantiomers *via* hindered rotation around the N–C_{aryl} bond [25-28]. The synthesis of atropisomeric compounds –molecules that bear a chiral axis rather than a stereogenic atom and have barriers to rotation that are high enough to allow isolation of enantiopure species– is of particular interest in many current studies. The best known atropisomeric systems are biaryl compounds with *ortho* substituents that hinder rotation and prevent racemization. Atropisomers are used as effective chiral catalysts enabling the transmission of chiral information during reactions [29]. Recent advances in this field include an effective method for the enantioselective construction of biaryl compounds devised by Thomson *et al.* [30]. Furthermore, Miller *et al.* have described a dynamic kinetic resolution of biaryl atropismers by peptide catalysis [31], and Cozzi *et al.* have applied organocatalysis to atroposelective reactions [32]. Moreover, in a combined experimental and computational study atropisomerism has been created by introducing *ortho* substituted aryl groups to peptoid backbones [33]. Nevertheless, Roussel *et al.* have claimed that internal rotation does not account for the trend in the activation barriers for some pyrimidine-2-thione derivatives, and has suggested a ring opening-ring closure mechanism rather than hindered rotation around the N–C_{aryl} bond [34].

In a comprehensive study, Dogan *et al.* investigated the interconversion between *SM* and *RP* enantiomers of *N*-(*o*-aryl)-4-hydroxy-5,5-dimethyl-2-oxazolidinone derivatives 3 (Figure 2.1) [11], and proposed a racemization that occurs through a "ring-chain-ring tautomerization" mechanism [11]. In order to clarify the mechanism, the interconversion of the collected enantiomer in ethanol was followed by HPLC and the activation barrier for the interconversion of *SM* to *RP* was reported as 25.3 kcal/mol [11]. The interconversion has been suggested to occur through an acyclic aldehyde intermediate formed via ring-

chain tautomerization. The aldehyde intermediate, although not observed in the NMR timescale in $CDCl_3$, was treated with benzyl amine in toluene and trapped in the form of an imine. The product was identified as a cyclic aminal structure formed by attack of the NH group to the formed imine. Thus the presence of the acyclic aldehyde intermediate was verified indirectly by ^{1}H and ^{13}C NMR characterization of the cyclic aminal product formed after its treatment with benzyl amine in toluene [11]. 2-oxazolidinone derivatives **3** are heterocyclic analogues of biphenyl atropisomers and have been found to be resolvable by HPLC on a chiral column. These separated enantiomers have the potential to be used as axially chiral catalysts [11]. Thus, it is imperative to gain more insight into their racemization modes, in order to be able to set the conditions where they remain stable as single enantiomers.

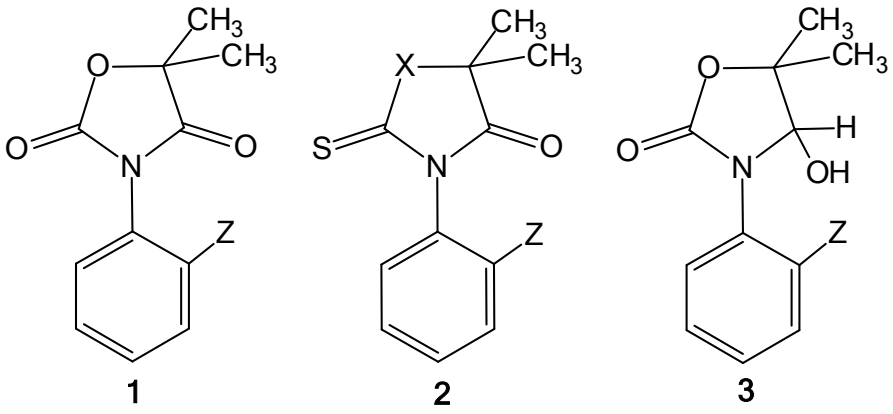

Figure 2.1. Structures of *N*-(*o*-aryl)-5,5-dimethyl-2,4-oxazolidinedione 1, *N*-(*o*-aryl)-5,5-dimethyl-rhodanine (X=S), oxazolidine-2-thiones (X=O) 2 and *N*-(*o*-aryl)-4-hydroxy-5,5-dimethyl-2-oxazolidinone derivatives 3 (Z=F, Cl, Br, I or Me).

On a purely experimental basis, it is difficult to assess the mechanism that governs the racemization process. However, theoretical methods have the potential to isolate various factors and, hence, a computational investigation on the mechanism of ring-chain-ring tautomerization in *N*-(*o*-tolyl)-4-hydroxy-5,5-dimethyl-2-oxazolidinone 3 (where Z=methyl) has been carried out by Density Functional Theory (DFT) calculations to get an in-depth understanding of the mechanism involved.

2.2. Computational Methods

Geometry optimizations and frequency calculations at the B3LYP/6-31+G(d,p) [35] level of theory were performed using Gaussian 03 and Gaussian 09 program packages [36, 37]. The intrinsic reaction coordinate (IRC) [38] for the ring-chain-ring tautomerization path was traced to connect the transition structures and the corresponding reactants and products. Zero point energies and thermal corrections were obtained from vibrational frequencies, which were also used to confirm the nature of the stationary points. Energy values for rotational barriers include thermal free energy corrections at 298.15 K and 1 atm, whereas those for the ring-chain-ring tautomerization mechanism were calculated at 323 K due to experimental conditions. The effect of a polar environment was taken into account via single point calculations by the use of the self-consistent reaction field (SCRF) [39] theory, utilizing the conductor like-polarizable continuum (CPCM) [40] model in ethanol. The UFF cavity model [41] in Gaussian 09 was used. Energy values for solvent calculations include thermal free energy corrections taken from gas phase optimizations. Single point energy calculations were carried out for all structures at the B3LYP [35], BMK [42], MPWB1K [43], MP2 [44], SCS-MP2 [45] and M06-2X [46, 47] levels using the 6-311+G(3df,2p) basis set on B3LYP/6-31+G(d,p) optimized structures. At each level of theory, the free energies include the thermal free energy corrections obtained from gas phase calculations at the B3LYP/6-31+G(d,p) level.))

2.3. Results and Discussion

2.3.1. Rotational Mechanism

The reduction of 1 with $NaBH_4$ at C4 is expected to form four stereoisomers (*RP*, *SM*, *SP* and *RM*) of 3 due to the new chiral center at C4 (Figure 2.2). The kinetic products (*SP* and *RM*) that form *via* the Felkin-Anh model [48] i.e. hydride attack at the *anti* direction of the *ortho* phenyl substituent, are converted to the thermodynamic products (*RP* and *SM*) via a fast rotation around the $N–C_{aryl}$ bond. As a result, the hydroxyl group at C4 and the *ortho* phenyl substituent are *antiplanar* with respect to each other (*RP* and *SM*) (Figure 2.2) [11].

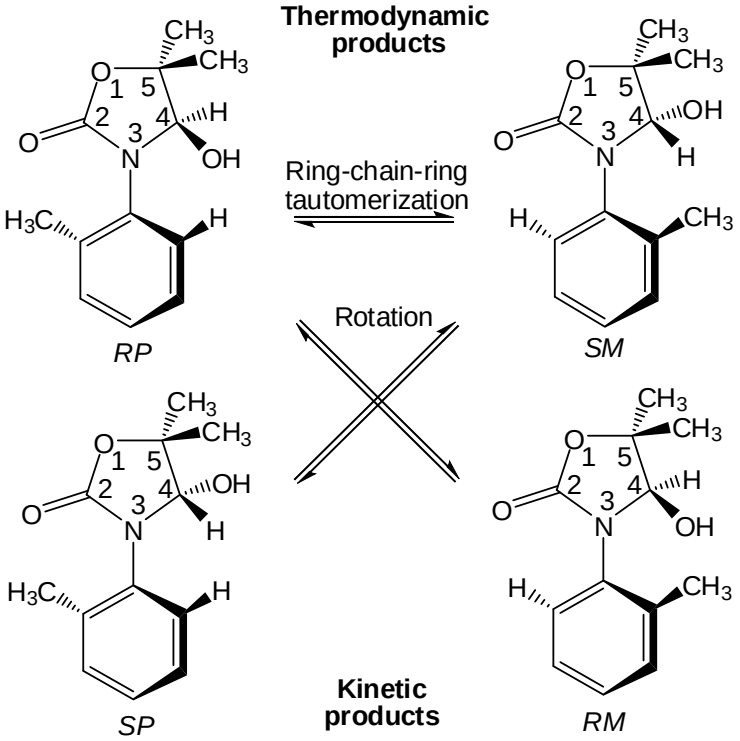

Figure 2.2. Rotation and ring-chain-ring tautomerization of 2-oxazolidinone 3.

Initially, the rotation around the N–C_{aryl} bond of 3 has been studied. The ground state configuration of *RP* and the corresponding rotational transition state between *RP* and *RM* are displayed in Figure 2.3. The rotational transition state (TS-Rot) around the N–C_{aryl} bond has a dihedral angle of $\theta_{a\text{-}b\text{-}c\text{-}d} = 180.3^{\circ}$, where the four atoms are planar. The ground state of *RP* is at $\theta = 71.3^{\circ}$. In the kinetically favored product (*RM*, $\theta = -72.7^{\circ}$) the methyl and the hydroxyl groups face each other and are in a sterically unfavorable orientation, thereby increasing the energy. We were also able to localize a second rotational transition state which is also quasi planar ($\theta = -2.8^{\circ}$), but it was found to be higher in energy (Figure 2.4) due to the lack of favorable interactions between the hydroxyl group at C4 and the methyl hydrogens of the *ortho*-phenyl substituent.

In *RP*, the lone pair of the hydroxyl oxygen has a favorable interaction with the methyl hydrogens at C5. In TS-Rot, methyl hydrogens at the *ortho* position of the ring repel the hydroxyl unit at C4, however, a favorable hydrogen bond between the hydroxyl group and the nitrogen is present (Figure 2.3). The same situation holds for the *SM*-*SP* pair.

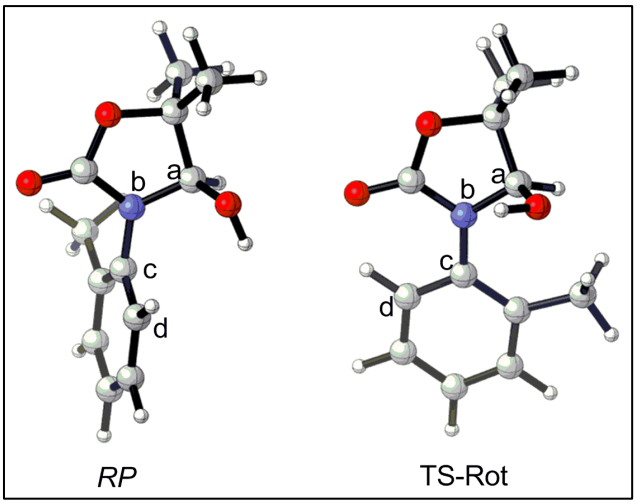

Figure 2.3. *RP* (lowest ground state) and TS-Rot (rotational transition state) of 2-oxazolidinone 3) (B3LYP/6-31+G(d,p)).

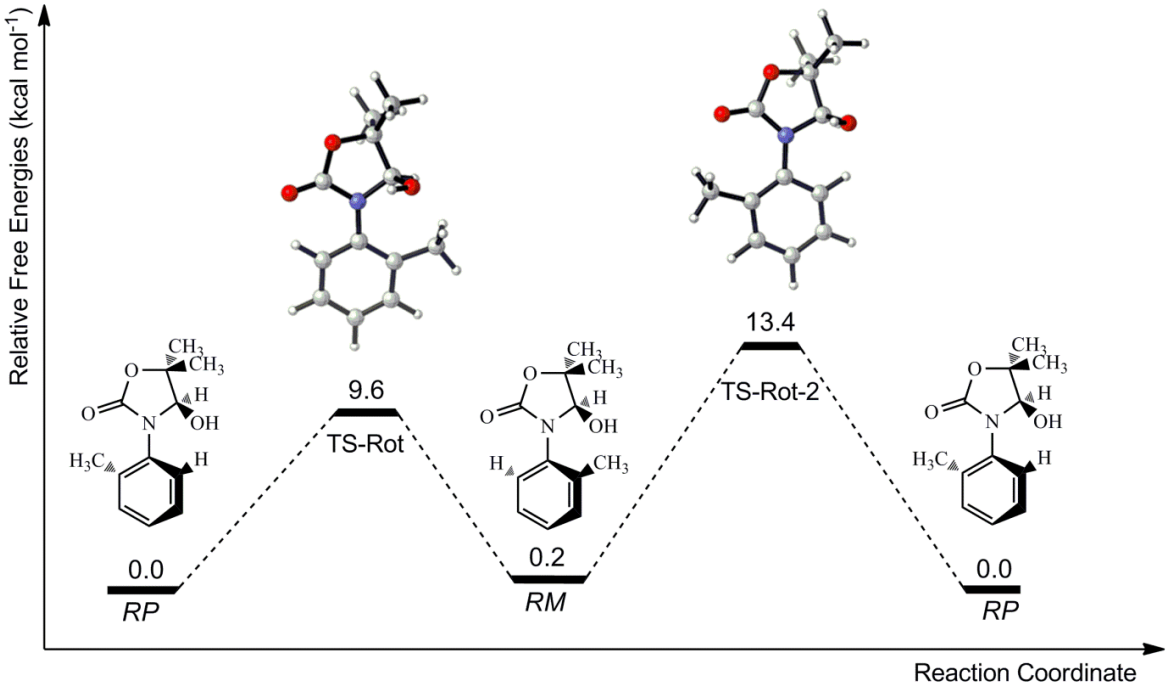

Figure 2.4. Rotational free energy profiles for *RP*-*RM* of N-(*o*-tolyl)-4-hydroxy-5,5-dimethyl-oxazolidinone (B3LYP/6-31+G(d,p)).

The results of the theoretical calculations for rotation are shown in Table 2.1. The experimentally hypothesized fast rotation is justified by the calculated low rotational barrier (ca. 10 kcal/mol), which leads to the formation of the thermodynamic products, *SM*

and *RP*. However, these rotational barriers do not correspond to the experimental barrier for tautomerization (25.3 kcal/mol) [11], moreover, rotation around the N–C_{aryl} bond cannot explain the experimentally observed interconversion of *SM* to *RP*.

Table 2.1. Rotational free energy barriers (298.15 K) at various levels of theory for 2-oxazolidinone 3.[a-c]

Method	$\Delta G^{\ddagger}_{\text{Rotation}}$ (kcal/mol)	
	RM-RP Rotation	*SM-SP* Rotation
B3LYP	9.4 [10.4]	9.6 [11.1]
BMK	9.2 [10.4]	9.3 [10.9]
M06-2X	9.0 [10.1]	9.2 [10.7]
MPWB1K	9.0 [10.1]	9.1 [10.7]
MP2	9.2	9.6
SCS-MP2	9.9	10.3

[a] Basis set: 6-311+G(3df,2p) [b] Values in brackets obtained from CPCM calculations with the same basis set. [c] Geometry optimizations: B3LYP/6-31+G(d,p)

2.3.2. Ring-chain-ring Tautomerization Mechanism

After the formation of the thermodynamic products, heating the resolved single *RP* enantiomer to 323 K converted it to its counterpart, *SM*. This was proposed to occur via the ring-opening of the heterocyclic ring followed by re-closure, since the interconversion between *SM* and *RP* cannot be achieved by a rotational mechanism. The ring-chain-ring tautomerization mechanism of *RP* to *SM* proceeds with N3–C4 bond breakage and leads to the formation of an acyclic aldehyde intermediate (Figure 2.5) [11]. The ring subsequently closes via the *Si* or *Re* face attack of the nitrogen leading to the formation of the corresponding enantiomer.

The interconversion of *RP* to *SM* by the ring-chain-ring tautomerization mechanism could, in principle, occur both via an amido and/or imino intermediate (Figure 2.5). Herein, we investigate, by means of theoretical calculations, the mechanistic details of the tautomerization pathway of 2-oxazolidinone 3 to elucidate whether the amido or imino intermediate occur and whether both pathways are possible.

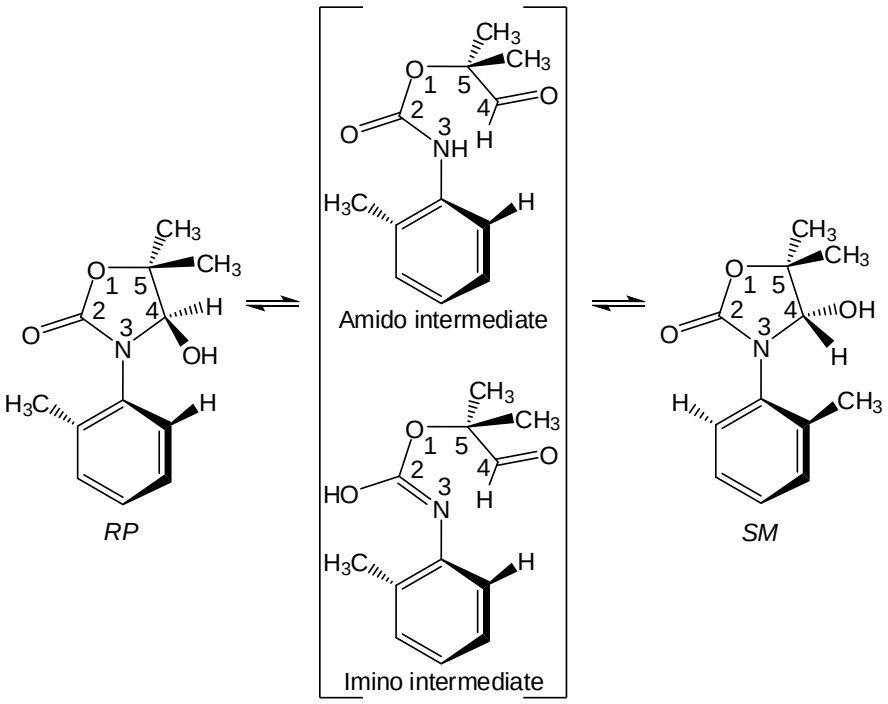

Figure 2.5. Ring-chain-ring tautomerization of 2-oxazolidinone 3 via an amido or an imino acyclic intermediate.

As the tautomerization takes place in ethanol, we investigated the effect of the environment by calculating the reaction profiles with and without the assistance of explicit solvent (ethanol) molecules. Bulk solvation effects were taken in to account as well.

Microsolvation –solvating with explicit solvent molecules– is extensively used in modeling reaction mechanisms, where the solvent plays a particular stabilizing role [49]. The use of solvent molecules in the assistance of the proton transfer steps, as in the case here, has proven to be crucial, since the solvent serves as the proton conduit [50-53]. Furthermore, several studies have shown that reactions involving the carbonyl functionality, such as peptidic amides, first interconvert to their more reactive tautomer counterparts; these tautomerization steps were also shown to be facilitated by polar protic solvents [50-53].

2.3.2.1. Ring-chain-ring Tautomerization Mechanism through Amido Intermediate. First, the amido mechanism (Figure 2.5) was investigated without the assistance of ethanol molecules. The potential energy surface for this pathway that illustrates the interconversion of *RP* to *SM* is displayed in Figure 2.6. The ground state *RP* yields the acyclic Amido intermediate 1 through the *RP* TS Amido No EtOH, in which bond breakage occurs by overcoming a barrier of 48.5 kcal/mol; this intermediate undergoes a rotation around the N–C_{aryl} bond and gives the Amido intermediate 2. In this step the *P* configuration of aryl ring changes to *M*, then rotation around the C4-C5 bond occurs, which yields the Amido intermediate 3 and the configuration of the stereocenter *R* changes to *S*. Note that all amido intermediates are plausible conformers of each other. Finally, ring closure occurs to yield the *SM* enantiomer. The two ground states (*RP* and *SM*) and the ring-opening, ring-closure transition states (*RP* TS Amido No EtOH and *SM* TS Amido No EtOH, respectively) are mirror images of each other (Figure 2.6).

The two rotational barriers are significantly lower than the first step in which bond rupture occurs, hence the ring-opening step for the *RP* enantiomer is identified as the rate determining step for the ring-chain-ring tautomerization. However, since the barrier for this step is unrealistically high, the effect of solvent assistance on this step has been explored. The transition state structures for the aforementioned ring-opening step are shown, with and without explicit (ethanol) molecules, in Figure 2.7. Visual inspection of the transition state structures clearly shows that the ring-opening step is prone to assistance by solvent bridges, in line with the Grotthus mechanism [54], which suggest proton transport occurs through molecular wires. The barriers for ring-chain-ring tautomerization, which correspond to the C4-N3 bond rupture, are summarized in Table 2.2 at various levels of theory. The assistance of protic ethanol molecules lowers the barrier on average by about 10 kcal/mol, but still the barriers remain too high by at least 10 kcal/mol compared to experimental values (25.3 kcal/mol).

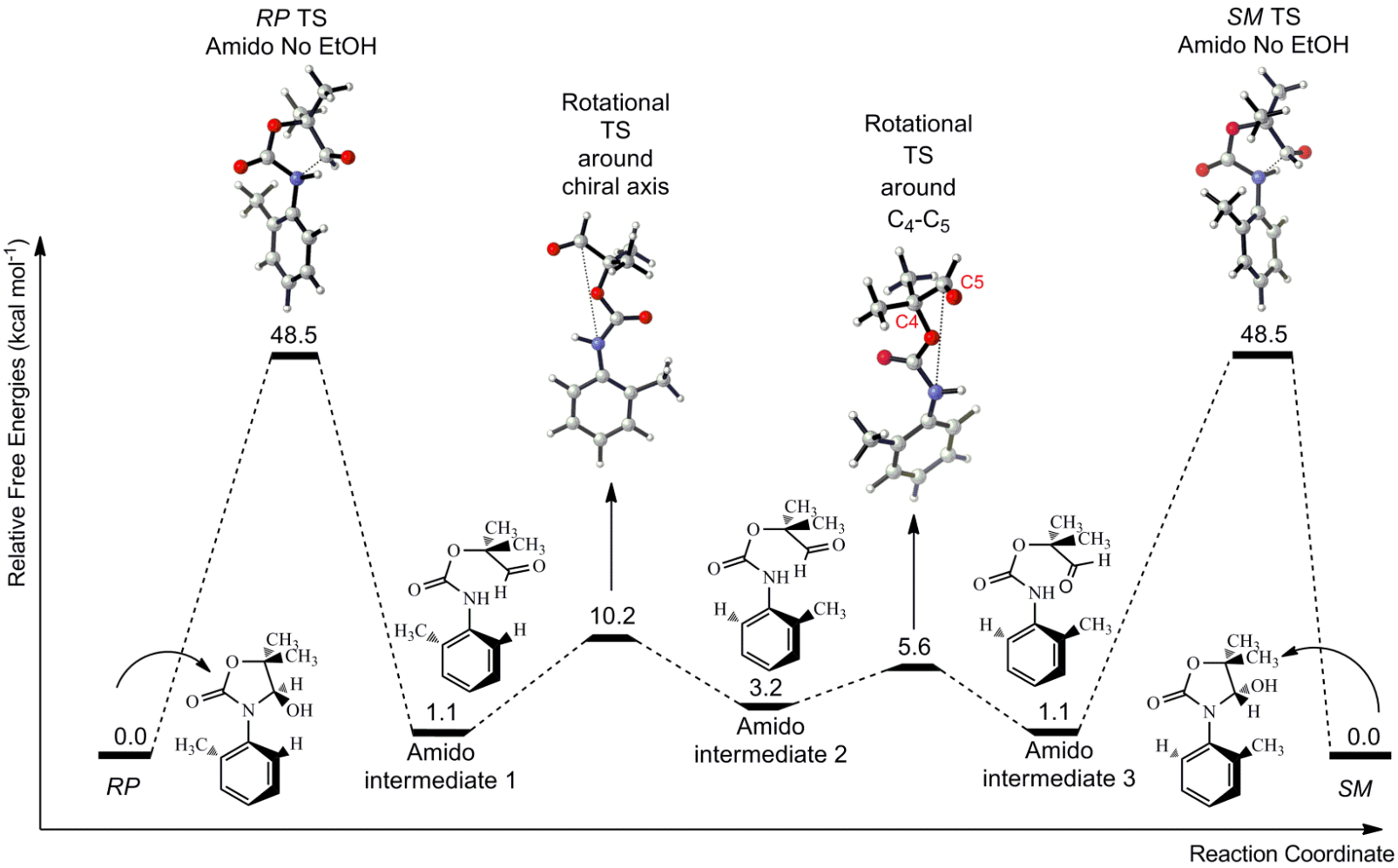

Figure 2.6. Potential energy surface for the ring-chain-ring tautomerzation of *RP* through an acyclic amido intermediate (B3LYP/6-311+G(3df,2p)//B3LYP/6-31+G(d,p)).

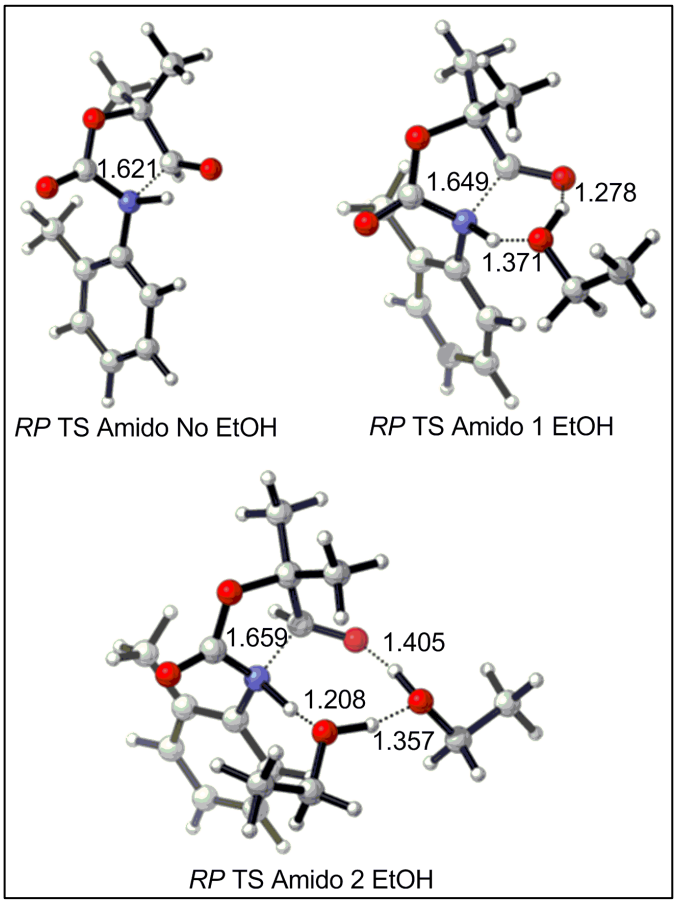

Figure 2.7. Optimized transition state geometries for ring-chain-ring tautomerization through "amido" acyclic intermediate (Critical distances given in Å.) (B3LYP/6-31+G(d,p)).

Table 2.2. Free energy barriers (323 K) at various levels of theory for the ring-chain-ring tautomerization for 2-oxazolidinone 3 through "amido" intermediate.[a-d]

Method	$\Delta G^{\ddagger}_{\text{Ring-opening}}$ (kcal/mol)		
	Amido No EtOH	Amido 1 EtOH	Amido 2 EtOH
B3LYP	48.5 [47.8]	37.3 [36.6]	39.7 [37.7]
BMK	50.8 [50.0]	40.3 [39.5]	41.4 [39.3]
M06-2X	51.4 [50.7]	37.5 [36.7]	36.0 [33.9]
MPWB1K	53.1 [52.3]	42.1 [41.3]	43.8 [41.7]
MP2	48.5	35.8	35.2
SCS-MP2	50.3	39.3	39.8
B3LYP-PCM opt.[e]	50.6 [49.9]	37.9 [37.1]	40.8 [38.9]

[a] Basis set: 6-311+G(3df,2p) [b] Values in brackets obtained from CPCM calculations with the same basis set. [c] Geometry optimizations: B3LYP/6-31+G(d,p) [d] Experimental value: 25.3 kcal/mol at 323 K. [e] These energies refer to PCM optimized geometries with B3LYP/6-31+G(d,p).

2.3.2.2. Ring-chain-ring Tautomerization Mechanism through Imino Intermediate. The interconversion of *RP* to *SM* was also explored through an "imino" form of the aldehyde intermediate, as shown in Figure 2.5. In case of the imino intermediate, it was impossible to locate the transition state without solvent assistance. This can easily be rationalized, by inspecting some critical distances between pairs of atoms involved in the reaction coordinate. In this case, the distance between the carbonyl oxygen at the C2 position and the hydroxyl group at C4 is too large (3.833 Å) to allow a direct proton transfer between these two centers. In the imino mechanism, one (*RP* TS Imino 1 EtOH) or two ethanol molecules (*RP* TS Imino 2 EtOH) act as a bridge in the proton transfer from the hydroxyl group at C4 to the carbonyl oxygen at C2 (Figure 2.8). Both the proton transfer and the C4-N3 bond cleavage occur simultaneously, leading to the formation of the acyclic imino structure. Subsequently, with the attack of N3 from the opposite side, the *SM* isomer forms. The assistance of two ethanol molecules for the formation of an acyclic imino intermediate further lowers the barrier to ring-opening (Table 2.3). At all levels of theory the ring-opening activation barrier with two ethanol molecules becomes remarkably close to the experimental value.

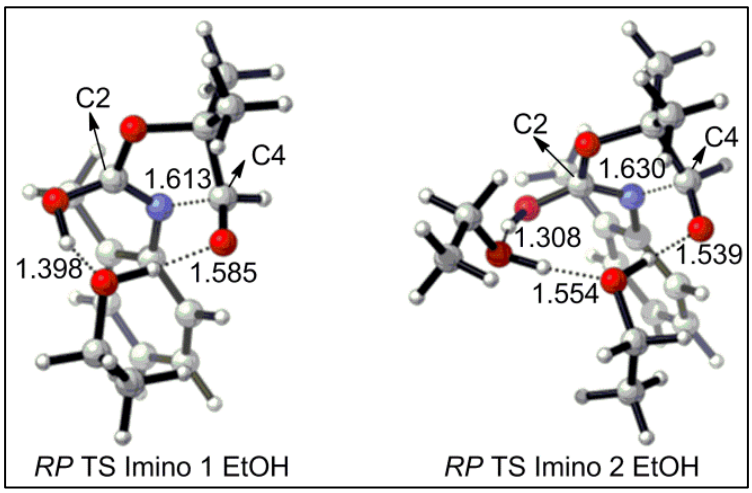

Figure 2.8. Optimized transition state geometries for ring-chain-ring tautomerization through "imino" acyclic intermediate (Critical distances given in Å.) (B3LYP/6-31+G(d,p)).

Table 2.3. Free energy barriers (323 K) at various levels of theory for the ring-chain-ring tautomerization for 2-oxazolidinone 3 through "imino" intermediate.[a-d]

Method	$\Delta G^{\neq}_{\text{Ring-opening}}$ (kcal/mol)	
	Imino 1 EtOH	Imino 2 EtOH
B3LYP	35.5 [36.3]	27.0 [26.8]
BMK	38.3 [39.0]	30.0 [29.7]
M06-2X	35.5 [36.1]	27.0 [26.6]
MPWB1K	38.2 [38.9]	31.0 [30.6]
MP2	35.6	27.5
SCS-MP2	39.2	30.8
B3LYP-PCM opt.[e]	36.7 [36.7]	29.7 [27.4]

[a] Basis set: 6-311+G(3df,2p) [b] Values in brackets obtained from CPCM calculations with the same basis set. [c] Geometry optimizations: B3LYP/6-31+G(d,p) [d] Experimental value: 25.3 kcal/mol at 323 K. [e] These energies refer to PCM optimized geometries with B3LYP/6-31+G(d,p).

Based on the perfect agreement between the theoretically determined free energy barriers (Imino mechanism 27 kcal/mol) and the experimental value (25.3 kcal/mol), it can be concluded that the ring-chain-ring tautomerization occurs via the imino mechanism. Hence, an overview of the entire pathway that corresponds to the *RP*–*SM* interconversion through the "solvent-assisted imino mechanism" and the corresponding potential energy surface is shown in Figure 2.9. In short, the ground state *RP* (*RP* 2 EtOH) undergoes ring opening to yield the acyclic Imino intermediate 1, which then gives Imino intermediate 3 by overcoming two rotational steps, as previously shown in Figure 2.6. Finally, the Imino intermediate 3 converts to the *SM* (*SM* 2 EtOH) by ring closure. Compared to the "non-assisted amido mechanism" (Figure 2.6), the rotational barriers for the imino mechanism with two ethanol molecules have been found to be slightly higher, however, it is again clearly seen that the rate determining step for the interconversion of *RP* to *SM* is the ring-opening step for the *RP* enantiomer, as expected.

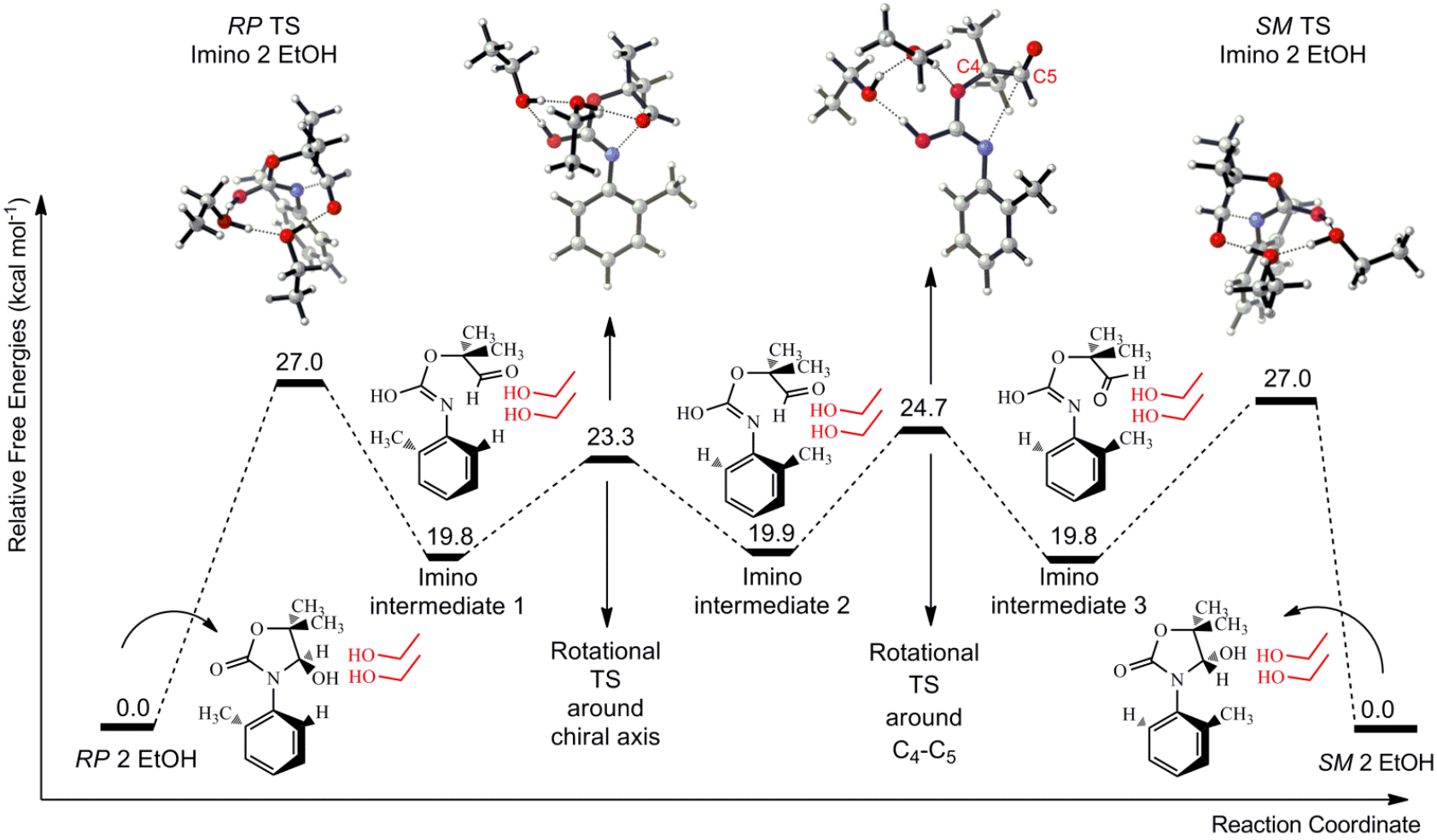

Figure 2.9. Potential energy surface for the ring-chain-ring tautomerzation of *RP* 2 EtOH through an acyclic imino intermediate (B3LYP/6-311+G(3df,2p)//B3LYP/6-31+G(d,p)).

The amido and imino forms of the acyclic intermediate, which are formed by the ring-opening of the *RP* enantiomer, are shown in Figure 2.10 with two solvating ethanol molecules. The main difference between these intermediates is the C2 atom and its substituents. In the amido intermediate 1 there is a carbonyl group at the C2 position, whereas in the imino intermediate 1 this center is in its corresponding enol form. The amido intermediate is the result of the proton transfer between the hydrogen atom at N3 and the carbonyl group at C4; the imino intermediate is the outcome of the proton transfer between the –OH group at C2 and the carbonyl group at C4. Solvent molecules are aligned to assist proton transfer. In the amido intermediate, the distance between N3 and C4 is 2.796 Å, whereas in the imino intermediate, it is 2.532 Å. Although the barriers leading to the imino intermediate are lower, the intermediate itself is slightly higher in energy than the amido intermediate (Table 2.4).

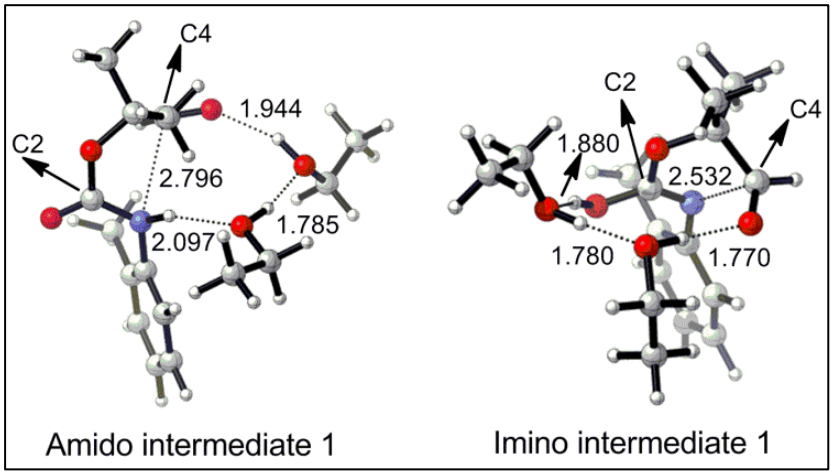

Figure 2.10. Amido and imino acyclic intermediate structures of 2-oxazolidinone 3 with two ethanol molecules (Critical distances given in Å.) (B3LYP/6-31+G(d,p)).

Table 2.4. Relative free energies of the amido and imino intermediates with/without solvent assistance in kcal/mol (B3LYP/6-311+G(3df,2p)//B3LYP/6-31+G(d,p)).

	Relative energies (kcal/mol)	
	No ethanol assistance	Two ethanol assistance
Amido intermediate	0.0	0.0
Imino intermediate	16.0	4.0

In order to gain more insight into the intermediate structures in Figure 2.6 and Figure 2.9, all obtained intermediate geometries are displayed in Figure 2.11. For the amido mechanism case, amido intermediate 1 is obtained from ring cleavage of *RP*, amido intermediate 2 differs from amido intermediate 1 by rotation around the chiral axis and when rotation around C4-C5 bond of amido intermediate 2 takes place, amido intermediate 3 forms. For imino mechanism case, the same story holds for formation of all intermediates but they also carry two ethanol molecules.

Amido Intermediate 1	**Amido intermediate 2**	**Amido intermediate 3**
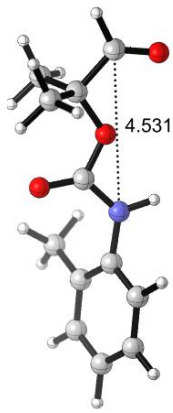	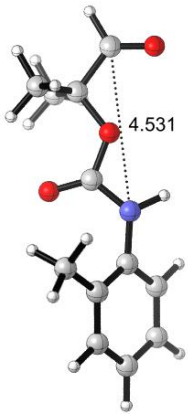	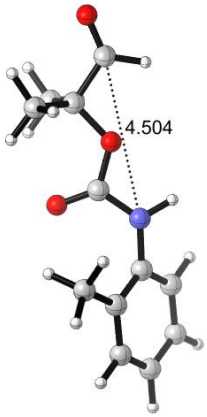
Imino intermediate 1	**Imino intermediate 2**	**Imino intermediate 3**
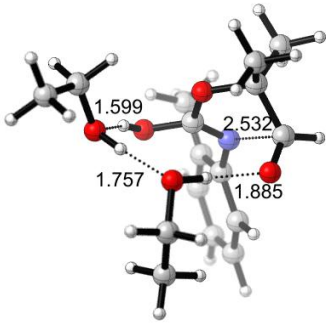	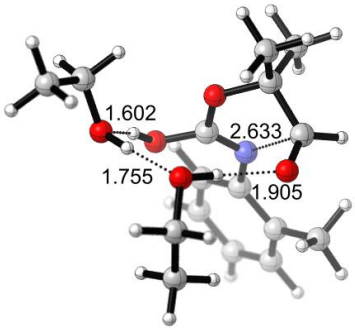	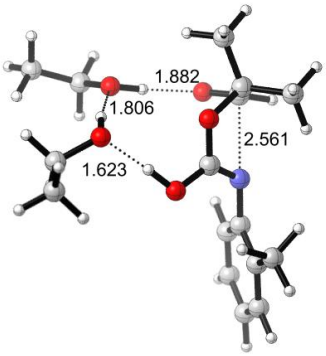

Figure 2.11. Geometries of amido intermediate 1, amido intermediate 2, amido intermediate 3 and imino intermediate 1, imino intermediate 2, imino intermediate 3 (B3LYP/6-31+G(d,p)) (Figure 2.6 and Figure 2.9) (Critical distances given in Å.).

2.4. Conclusions

In this study, the enantiomeric interconversion observed for 2-oxazolidinone derivatives **3** –heterocyclic analogues of biphenyl atropisomers with potential to be used as axially chiral catalysts– has been theoretically assessed; the mechanism of their interconversion as well as the environmental factors that contribute to their racemization has been thoroughly elucidated.

This study has shown that the *SM* and *RP* enantiomeric pairs of N-(*o*-tolyl)-4-hydroxy-5,5-dimethyl-2-oxazolidinone 3 interconvert to each other through a ring-chain-ring tautomerization mechanism. An acyclic aldehyde intermediate was previously suggested, although not experimentally isolated; this study reveals that the ring-chain-ring tautomerization occurs through an 'imino intermediate' rather than an 'amido intermediate'.

Solvent effects were found to be essential in the reaction mechanism, since proton hopping is facilitated by the presence of assisting ethanol molecules, in line with the proton transport suggested for hydrogen-bonded solvents in the Grotthus mechanism [54]. While kinetic functionals, BMK [42] and MPWB1K [43], slightly overestimated the ring-opening barrier, M06-2X [46, 47], known to perform well in organic systems with dispersive effects [49, 55], showed results that are consistent with experimental findings.

Summarizing, this theoretical study sheds light on the conditions where 2-oxazolidinone derivatives 3, which are potential chiral catalysts, remain stable as single enantiomers. The role of the solvent is crucial in the racemization process; hence, the use of aprotic solvents will likely suppress racemization. This information will prove very useful for similar heterocyclic analogues of biphenyl atropisomers that are used as axially chiral catalysts.

3. ASYMMETRIC DESYMMETRIZATION OF *MESO* ANHYDRIDES WITH CINCHONA ALKALOIDS

3.1. Introduction

Cinchona alkaloids have demonstrated widespread potentiality in the field of chiral molecular recognition, and have been successfully employed as chiral catalysts in asymmetric processes [56-58]. Their versatility is commonly attributed to the presence of several functionalities and their ability to act as multisite receptors. To understand the molecular basis of their strong performance, several conformational investigations have been carried out both with computational and NMR methods [59-63]. Assessing the dynamics of cinchona alkaloids is important in developing a comprehensive understanding of the mechanisms of enantiodifferentiation in catalytic reactions.

The family of cinchona alkaloids consists of two pseudoenantiomeric pairs, cinchonine-cinchonidine and quinine-quinidine (Figure 3.1). Cinchona alkaloids consist of two rigid moieties, a quinoline ring which is the aromatic system and a quinuclidine ring which is the bicyclic ring system, coupled together by two carbon-carbon bonds.

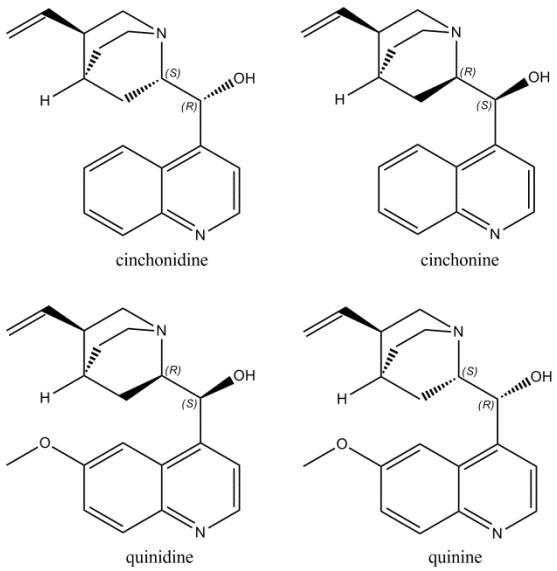

Figure 3.1. The derivatives of cinchona alkaloids.

The relative position of the quinoline and quinuclidine rings determines the conformational diversity of the alkaloid. Mainly, the cinchona alkaloids are found in open and closed conformations. In open conformation, the lone pair of electrons on the quinuclidine N points away from the quinoline ring, whereas it points towards the quinoline ring in closed conformation (Figure 3.2).

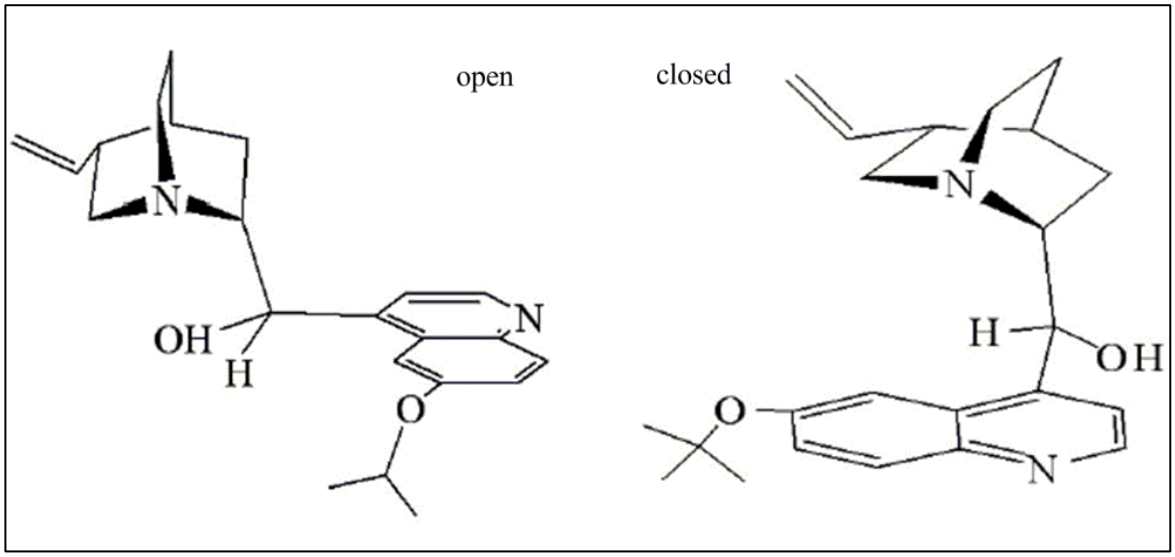

Figure 3.2. Open and closed conformations of quinidine.

The first non-enzymatic process of asymmetric desymmetrization with cinchona alkaloids has been performed by Oda and co-workers in 1985 [64] They have found that asymmetric desymmetrization (AD) reaction of cis-dimethylglutaric anhydride can be carried out with cinchona alkaloids [64]. Then Aitken and co-workers have reported that conversion of *meso* epoxy anhydride to a lactone can be catalyzed by cinchonine [65]. In 1999, Bolm and co-workers built upon the findings reported by the groups of Oda and Aitken to develop a more enantioselective methanolysis protocol mediated by quinidine [66] Both enantiomers can be easily obtained with up to 98% enantiomeric excess by using either quinine or quinidine in that case. These reported procedures are summarized in Figure 3.3.

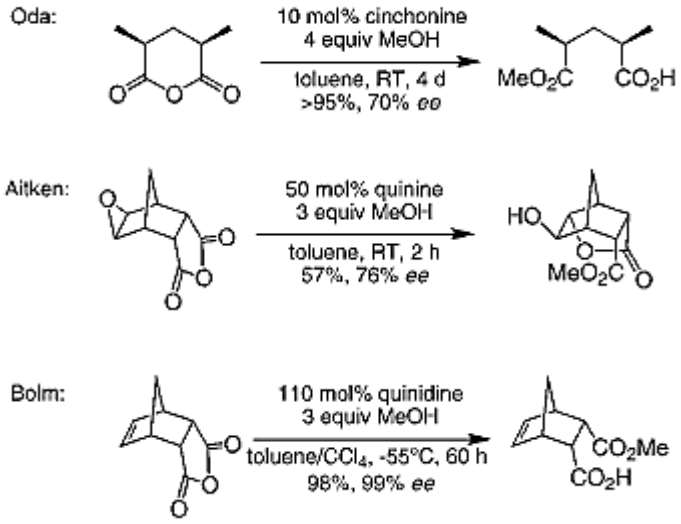

Figure 3.3. Reactions which are catalyzed by cinchona alkaloids [64-66].

After various studies, it has been proposed that there are two possible mechanisms for the asymmetric desymmetrization of cyclic anhydrides these are nucleophilic and general base catalysis [22, 64, 65] In nucleophilic catalysis, the nucleophilic attack by the amine nitrogen on the anhydride forms a reactive chiral acylammonium salt. Nucleophilic attack on this salt by the secondary alcohol gives the ester product and regenerates the amine. Aitken and Bolm claim that the mechanism that operates for cyclic anhydride ring opening is the nucleophilic one. However, in the general base catalysis as proposed by Oda and co-workers the cinchona catalyzed ring-opening of *meso* anhydrides involves the quinuclidine nitrogen acting as a chiral general base rather than a nucleophile. Both mechanisms are shown in Figure 3.4. Recently, it has been demonstrated that the general base catalysis is preferred over the nucleophilic catalysis for AD of *meso* anhydrides with catalysts such as amino alcohols [67]. This finding has been extrapolated to the fact that the AD of *meso* anhydrides with quinine-quinidine pseudoenantiomeric pairs also occurs through general base catalysis mechanism.

In this study, the alcoholysis of *meso* anhydrides in the presence of quinine and quinidine (Figure 3.5) has been subjected to quantum chemical calculations in order to gain insight into the mechanism. The conformational analysis of quinine-quinidine pseudoenantiomeric pairs has been performed to find the best conformations which then have been used to model the mechanisms. Bolm and co-workers have reported that addition of methanol to the anhydride 1 in the presence of quinidine yields the product 2,

whereas quinine, the pseudoenantioner of quinidine, generates *ent*-2 with the same enantiomeric excess [68]. The general base catalysis pathway has been explored for these addition reactions in the presence of both cinchona catalysts, quinidine and quinine. The effect of the solvent to the reactions has been also examined.

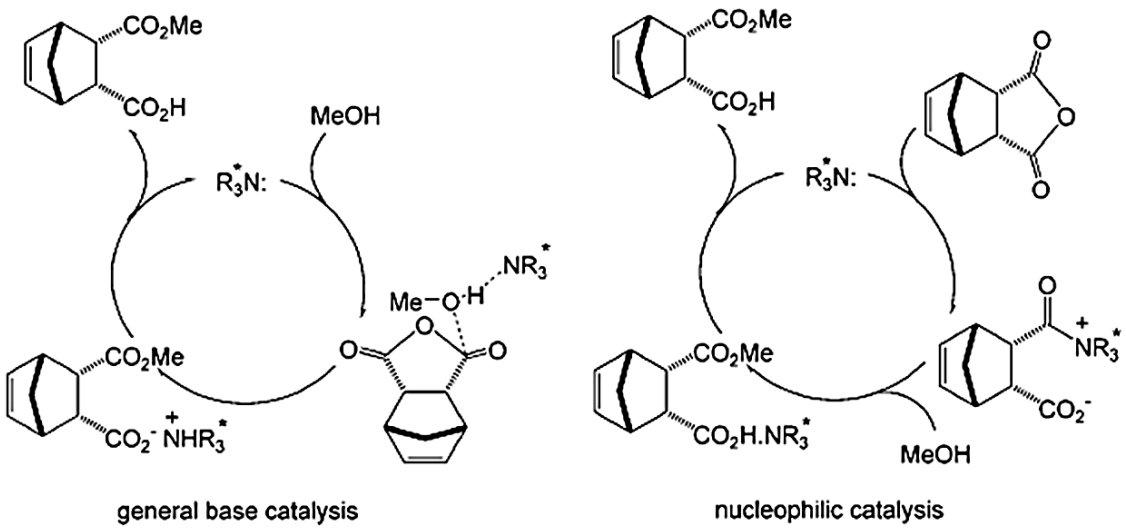

Figure 3.4. The general base and nucleophilic catalysis of ring opening of meso cyclic anhydrides.

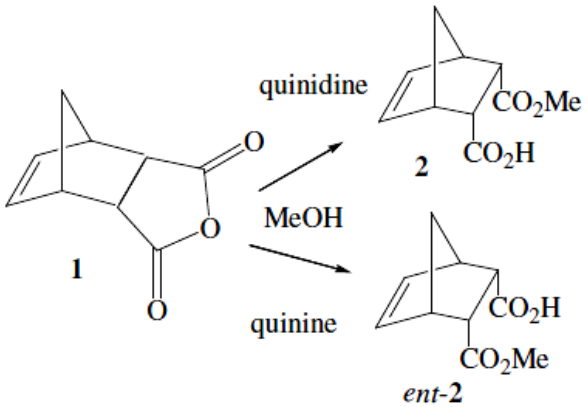

Figure 3.5. Asymmetric desymmetrization of 1 with cinchona alkaloids [68].

3.2. Computational Methods

All gas phase geometry optimizations were performed using the Density Functional Theory [69] at the B3LYP/6-31+G(d,p) level of theory [35]. Single point calculations with

M06-2X/6-31+G(d,p) [46, 47] have also been carried out for the energy refinements. The intrinsic reaction coordinate (IRC) [38] was used to connect the transition structures and the corresponding reactants and products. Zero point energies and thermal corrections were obtained from vibrational frequencies. At each level of theory, the free energies include the thermal free energy corrections obtained from gas phase calculations at the B3LYP/6-31+G(d,p) level at 298.15 K and 1 atm. The effect of a polar environment was taken into account by use of Self Consistent Reaction Field Theory (SCRF) [39], utilizing the Integral Equation Formalism Polarizable Continuum Model (IEFPCM) [70] in toluene (ε= 2.3741) which is the solvent used in the experiments. The UFF cavity model [41] was used. All the calculations were carried out using Gaussian 09 program package [37].

3.3. Results and Discussion

3.3.1. Conformational Analysis of Cinchona Alkaloids

Due to variety of the reactions that the cinchona alkaloids can promote, the availability of both enantiomeric antipodes in large quantities from most chemical suppliers and their stability, they are widely used as catalysts in synthetic chemistry [56-58]. In asymmetric processes, their addition to the reaction provides the enantioselectivity that results from the specific interaction between the alkaloid and the reactant molecule which mainly depends on the specific conformation of the alkaloid: the conformation of the alkaloid plays a crucial role in determining the chirality of the product. Due to this important role, there have been many studies on the conformational behavior of cinchona alkaloids in the literature [59-63]. It has been found that there are three significant dihedral angles τ_1, τ_2 and τ_3 which determine the conformation of the alkaloid and they are shown in Figure 3.6. τ_1 represents the dihedral angle $C_1 - C_2 - C_3 - C_4$; τ_2 represents the dihedral angle $C_2 - C_3 - C_4 - C_5$ and τ_3 is the dihedral angle $H_3 - C_3 - C_4 - H_4$.

After reporting the most stable conformations of the cinchona alkaloids-open and closed conformations- in 1998 Baiker *et al.* have investigated all the conformations of cinchonidine and found several stable conformations [59]. According to NMR and ab initio calculations, Open(3), Closed(1) and Closed(2) conformations have been found to be the

most stable conformations and Open(3) is the most stable one among these conformations in apolar solvents. However, when the polarity of the solvent increases, Closed(1) and Closed(2) conformations become more stabilized mainly due to their larger dipole moments. Overall, it has been suggested that Open(3) plays a crucial role in enantiodifferentiation [59]. In 2008, the same group has found additional stable conformers of cinchonidine by a combined NOESY-DFT analysis [63]. According to this study, Closed(7) and Open(10) conformations are also stable as the previously found conformations. All the conformations of cinchonidine are displayed in Figure 3.7 and their important dihedral angles and relative energies are summarized in Table 3.1.

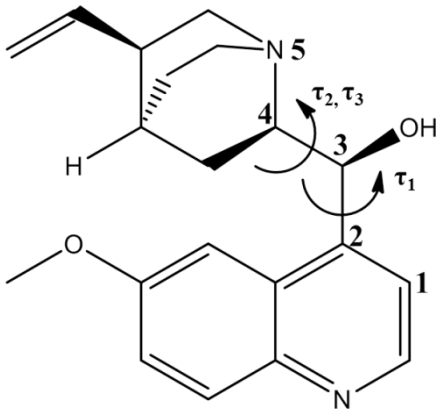

Figure 3.6. τ_1, τ_2 and τ_3 dihedral angles.

Table 3.1. Characteristic dihedral angles and relative energies (RE) (kcal/mol) of the various conformations of cinchonidine [63].

BLYP-PW				
Cinchonidine	**τ_1**	**τ_2**	**τ_3**	**RE**
Closed(1)	248.9	50.1	175.0	1.11
Closed(2)	60.1	59.9	180.1	1.45
Open(3)	98.7	150.1	278.2	0.00
Open(4)	260.2	139.7	271.8	2.57
Open(5)	88.4	310.5	76.0	5.02
Open(6)	260.1	309.8	78.5	4.90
Closed(7)	17.3	52.8	172.7	1.29
Open(8)	20.0	149.8	277.9	2.29
Open(9)	10.1	270.0	41.9	6.07
Open(10)	101.8	267.7	37.7	1.31
Open(11)	279.2	272.5	46.4	3.87

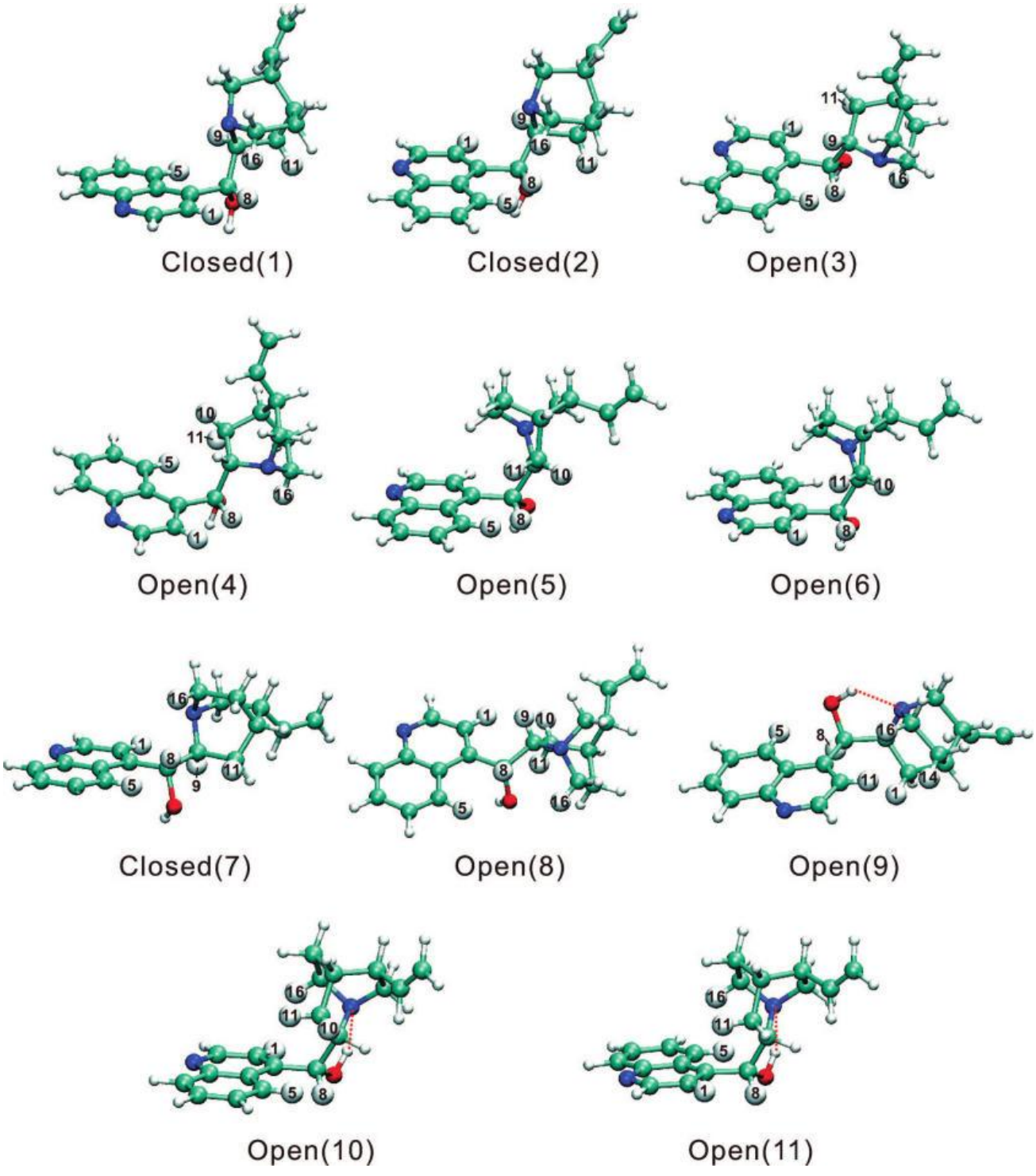

Figure 3.7. Minimum energy conformations of cinchonidine with BLYP-PW method [63].

Because the conformation of the cinchona alkaloid has a very important role in enantiodifferentiation, the conformational analysis of quinine and quinidine has been carried out in details. The characteristic dihedral angles of 11 conformations of cinchonidine have been applied both to quinine and quinidine and the obtained geometries have been optimized with the method used in this study. Since cinchonidine and quinine have chiral carbons with same stereochemistry (Figure 3.1) and the only difference between them is the presence of the methoxy group attached to the quinoline ring in quinine, the characteristic dihedral angles were applied directly to quinine. However, as the differences between cinchonidine and quinidine are not only the presence of the methoxy group but also the opposite stereochemistry at their chiral carbons (Figure 3.1), dihedral angles of cinchonidine could not be directly applied to quinidine. If the presence of methoxy group is ignored, cinchonidine and quinidine can be treated as pseudoenantiomeric pairs, thus kind of mirror images of each other. At this point, characteristic angles of cinchonidine were converted to new angles that fit the quinidine structure by subtracting them from 360 degrees since they have opposite stereochemical properties. Therefore, the characteristic dihedral angles of cinchonidine were first subtracted from 360 degrees and then were applied to quinidine structure in order to obtain the proposed conformations. The newly obtained characteristic dihedral angles of quinine and quinidine and their relative energies are given in Table 3.2. For both quinidine and quinine, the most stable conformer has been found to be Open(3) as proposed in previous studies. Closed(1), Closed(2), Closed(7) and Open(4) conformations are the other most stable conformers for quinine. The suggested Open(10) conformation has been found to be 5.12 kcal/mol energetically higher than Open(3), hence it doesn't rank among the first five most stable conformers. Instead of Open(10), Open(4) has been found to be relatively lower in energy. For the quinidine case, the trend of the conformations is totally different. Firstly, it has been observed that all of the proposed conformations could not be obtained for quinidine, because the Open(8) conformation which differs from Open(3) with only τ_1 dihedral angle (Table 3.1) could not be located, it converted to Open(3) conformation as can be seen in Table 3.2. So, based on the relative energies of the obtained conformations, Open(5), Open(10), Closed(2) and Open(4) conformations are the ones that follow Open(3). It seems that Open conformations are more preferable than the Closed conformations for quinidine.

Table 3.2. Characteristic dihedral angles and relative energies (RE) (kcal/mol) of the conformations of quinine and quinidine.

B3LYP/6-31+G(d,p)									
Quinine	**τ_1**	**τ_2**	**τ_3**	**RE**	**Quinidine**	**τ_1**	**τ_2**	**τ_3**	**RE**
Closed(1)	251.2	56.2	181.8	1.18	**Closed(1)**	107.1	299.3	173.4	3.08
Closed(2)	72.8	60.8	183.0	1.32	**Closed(2)**	285.8	300.1	178.0	2.33
Open(3)	99.2	157.7	285.6	0.00	**Open(3)**	261.2	204.5	76.8	0.00
Open(4)	268.1	148.5	280.7	2.82	**Open(4)**	92.2	211.9	79.8	2.70
Open(5)	83.2	314.6	79.1	5.13	**Open(5)**	260.1	87.9	318.5	1.85
Open(6)	260.5	304.8	73.7	5.49	**Open(6)**	84.9	87.0	313.5	4.67
Closed(7)	20.2	54.3	175.4	1.56	**Closed(7)**	345.1	302.7	181.1	3.26
Open(8)	21.8	151.1	279.2	3.10	**Open(8)**	261.2	204.5	76.8	0.00
Open(9)	7.5	271.1	43.0	8.29	**Open(9)**	352.2	89.4	317.6	9.02
Open(10)	83.2	314.6	79.0	5.12	**Open(10)**	260.1	87.9	318.5	1.85
Open(11)	260.4	304.8	73.7	5.49	**Open(11)**	84.9	87.0	313.5	4.67

The calculated geometrical parameters of quinine have been compared with previously the findings of cinchonidine as their stereochemistry is the same. When the characteristic dihedral angles of cinchonidine obtained with the BLYP-PW method and the characteristic dihedral angles of quinine obtained with the B3LYP/6-31+G(d,p) method are compared, it is seen that they do not change too much and therefore the relative energy trend of the conformations is almost the same except for the ranking interchange of Open(4) with Open(10). Based on the quinine conformations, the percent deviations of the τ_1, τ_2 and τ_3 dihedral angles from the corresponding cinchonidine angles (Table 3.1) have been also calculated. These deviations and their averages are summarized in Table 3.3. It seems that deviations of all conformations are within a range that proves there is no significant change except for Open(10) and Open(11).

Table 3.3 Percent deviations of τ_1, τ_2 and τ_3 dihedral angles of quinine from corresponding angles of cinchonidine.

Percent Deviations of Quinine			
Conformation	**τ_1**	**τ_2**	**τ_3**
Closed(1)	0.9	12.2	3.9
Closed(2)	21.1	1.5	1.6
Open(3)	0.5	5.1	2.7
Open(4)	3.0	6.3	3.3
Open(5)	5.9	1.3	4.1
Open(6)	0.2	1.6	6.1
Closed(7)	16.8	2.8	1.6
Open(8)	9.0	0.9	0.5
Open(9)	25.7	0.4	2.6
Open(10)	18.3	17.5	109.5
Open(11)	6.7	11.9	58.8
Average	9.8	5.6	17.7

According to the results of the conformational analysis of quinine and quinidine, the Open(3) geometry has been selected to be used in modeling the asymmetric desymmetrization mechanism of *meso* anhydrides. In addition, the choice of the Open(3) conformation has also been supported by the fact that the experimental solvent is toluene which is non-polar and Open(3) has been found to be more stabilized than closed conformations in apolar media which has been explained by larger dipole moments of closed conformations which have been obtained as 2.61 D and 2.89 D respectively, as compared to Open(3) whose dipole moment has been found to be 1.84 D [59]. The Open(3) conformations of both quinine and quinidine which are used in the next step of the study are displayed in Figure 3.8. As expected, the quiniclidine N points away from the quinoline ring for both pseudoenantiomers. In addition, when their characteristic dihedral angles are considered, the sum of each dihedral angle of quinine and quinidine is equal to approximately 360 degrees which results in being like a mirror image of each other as shown in Figure 3.8.

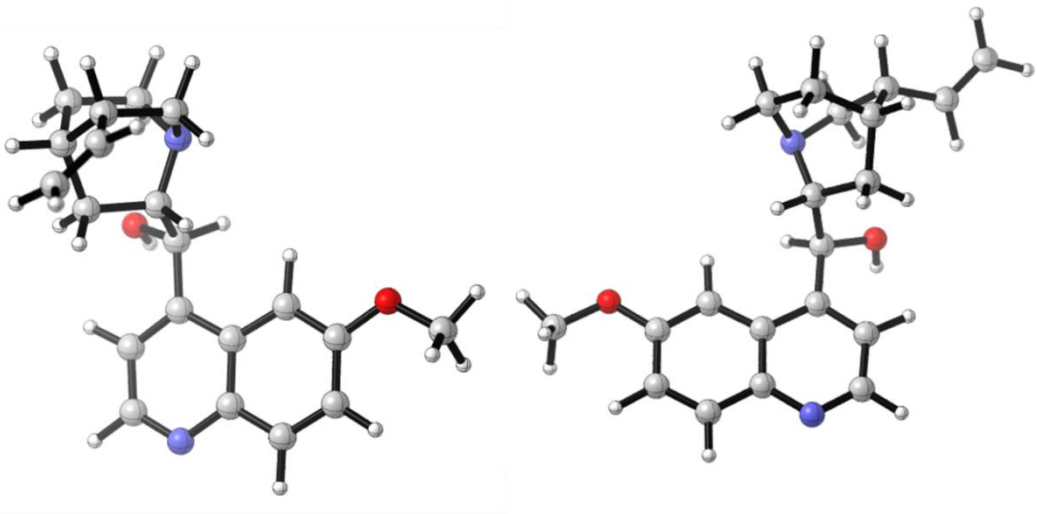

Figure 3.8. Open(3) conformations of quinine and quinidine (B3LYP/6-31+G(d,p)).

3.3.2. Asymmetric Desymmetrization Mechanism

The next step of the study is to model the base catalysis mechanism of asymmetric desymmetrization of *meso* anhydrides with quinine and quinidine. As mentioned earlier, the cyclic *meso* anhydride 1 has yielded experimentally the product 2 in the presence of quinidine whereas product ent-2 is formed when quinine is used as catalyst with up to 99% of enantiomeric excess as shown in Figure 3.9 [68]. In this part of the study, the addition of methanol to *meso* anhydride has been modeled in the presence of both quinine and quinidine, both concerted and stepwise pathways have been considered and modeled.

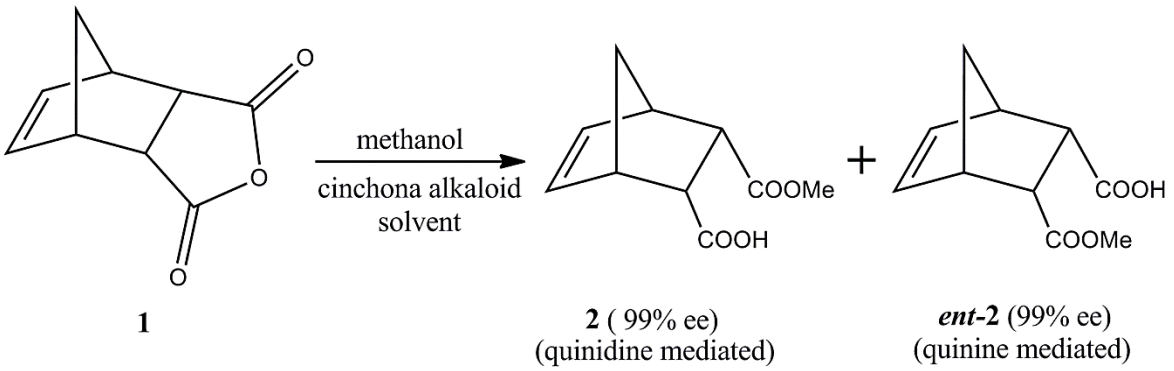

Figure 3.9. Addition of methanol to 1 with cinchona alkaloids [68].

3.3.2.1. Concerted Mechanism. In this mechanism, the addition of methanol to *meso* anhydride in the presence of cinchona alkaloids and opening of the ring yields the hemi-ester product, namely asymmetric desymmetrization, takes place in a single step.

First the methanol addition to *meso* anhydride 1 has been explored in the presence of quinidine. Although it is known that quinidine catalyzed reaction yields 2, both reaction pathways of which products are 2 and *ent*-2 have been modeled and their barriers have been calculated to compare with the experimental findings. The first step was locating the two transition states one of which gives the product 2 and the other yields *ent*-2. The difference between the two transition states is side of approach of methanol as displayed in Figure 3.10. If the methanol attacks the left carbonyl carbon of the anhydride, the product will be 2; if the methanol attacks the right side, the product will be *ent*-2.

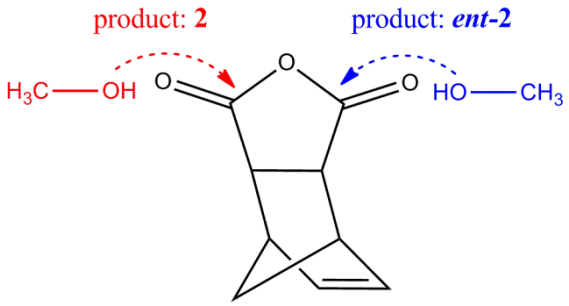

Figure 3.10. Addition of methanol to *meso* anhydride 1.

In both cases the Open(3) conformation of the quinidine has been used. In both transition states, the oxygen of methanol attacks the carbonyl carbon; the bond between the carbonyl carbon and the anhydride oxygen breaks and the quinuclidine nitrogen (N) of the quinidine assists the proton transfer from methanol to the carbonyl oxygen (Figure 3.11). The role of cinchona alkaloid is not limited to assisting the proton transfer; it also stabilizes the system with its hydroxyl group which forms a hydrogen bond with the oxygen of the other carbonyl group. The anhydride whose left carbonyl carbon is exposed to methanol attack (TS-QD-left) is stabilized by a hydrogen bond between the hydroxyl group of the quinidine and the right carbonyl oxygen of the anhydride with 1.84 Å distance. For the other case where methanol attack takes place from the right side of the anhydride (TS-QD-right), stabilization is due to the hydrogen bond between the hydroxyl group of the quinidine and left carbonyl oxygen with 1.86 Å distance. In both transition states, the critical distance

between the carbonyl carbon and the anhydride oxygen is around 1.5 Å. During the location of the transition states, an additional transition state structure has been located for the right methanol attack. This transition state is similar to TS-QD-right except for the location of the hydrogen bond. In this structure, the hydroxyl group of the quinidine makes hydrogen bond with the anhydride oxygen (TS-QD-right2) with 1.96 Å distance as shown in Figure 3.11. This type of transition state could not be located for the left attack since the structure of the quinidine does not allow doing it.

From the intrinsic reaction coordinate (IRC) calculations, the corresponding reactants and products have been located for quinidine catalyzed system. 3 reactants have been obtained from the 3 located transition states which are different conformations of each other. However, only one conformation of the reactants which is the most stable one has been taken into account during the calculations of activation barriers of the reactions. In addition, IRC analysis proved that TS-QD-left connects to product 2; TS-QD-right and TS-QD-right2 yield *ent*-2 as expected.

The calculated activation barriers of the asymmetric desymmetrization of *meso* anhydride **1** in the presence of quinidine have been summarized in Table 3.4. The characteristic dihedral angles of quinidine in the transition state structures have been also reported in Table 3.4 and it has been found that the dihedral angles are almost same with the angles of the previously located Open(3) conformation of quinidine (τ_1: 261.2, τ_2:204.5, and τ_3:76.8) which indicates that quinidine has preserved its Open(3) conformation in the transition state structures.

Table 3.4. Gibbs free energy barriers ($\Delta G^{\ddagger}$) of asymmetric desymmetrization of meso anhydride 1 with quinidine and characteristic dihedral angles of quinidine.

TS	**Product**	**Quinidine**			**$\Delta G^{\ddagger}$ (kcal/mol)**	
		τ_1	**τ_2**	**τ_3**	**B3LYP/6-31+G(d,p)**	**M06-2X/6-31+G(d,p)[a]**
TS-QD-left	**2**	256.7	198.9	69.8	21.3	17.1
TS-QD-right	***ent*-2**	254.3	194.5	66.8	24.2	25.7
TS-QD-right2	***ent*-2**	255.6	190.1	62.4	23.7	19.8

[a]The values are obtained from single point energies on the B3LYP/6-31+G(d,p) optimized geometries

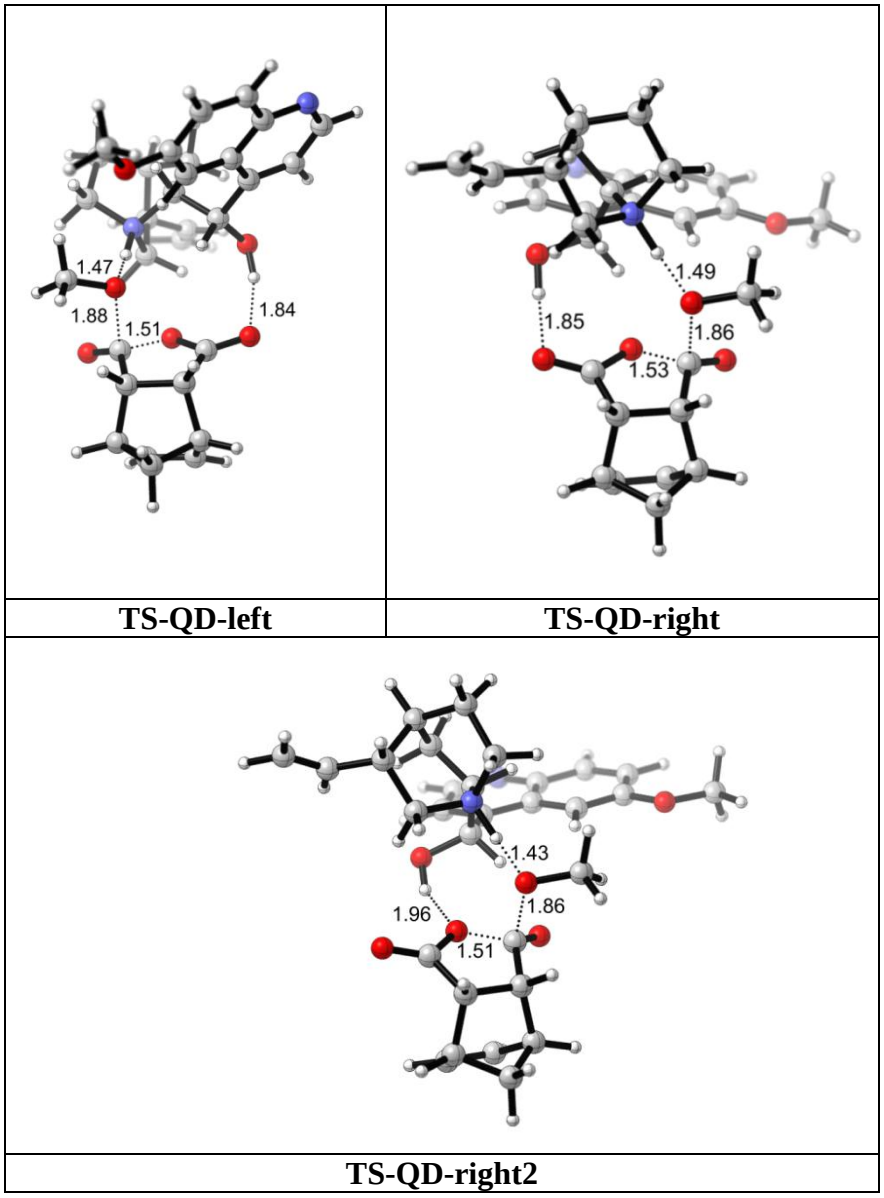

TS-QD-left	TS-QD-right

TS-QD-right2

Figure 3.11. Quinidine catalyzed transition state structures.

The activation barrier of the reaction whose product is 2 is ~ 2 kcal/mol lower than the one for the other reactions that yield product *ent*-2 according to both methods (Table 3.4). This result is in accordance with the experimental findings; since it is known that quinidine catalyzed reaction gives the product 2 enantioselectively [68]. Comparison of the activation barriers of TS-QD-right and TS-QD-right2 asserts that the hydroxyl group of quinidine prefers to make hydrogen bond with the anhydride oxygen than the left carbonyl oxygen in reaction yielding *ent*-2. Hence, TS-QD-left and TS-QD-right2 should be considered to discuss the energy barrier difference between the reaction of 2 with *ent*-2. When charges of the methanol oxygen and the carbonyl carbon to be attacked in these

transition structures are taken into account, the charge distribution between these atoms has been found to be better in TS-QD-left (C: -0.912 and O: -0.435) than TS-QD-right2 (C: -1.219 and O: -0.351) structure which can be the reason of energy difference between these transition state structures. This difference is about 2.4 kcal/mol according to B3LYP, whereas it is 2.7 kcal/mol with M06-2X method. On the other hand, M06-2X results are lower than the ones obtained from B3LYP which can be due to the fact that M06 functional performs better in estimating noncovalent interactions such as hydrogen bonds [46, 47]. Overall, it can be deduced that the quinidine catalyzed reaction yielding 2 is energetically preferred and this result is consistent with experimentally determined enantioselectivity [68].

The next step was to model the asymmetric desymmetrization of *meso* anhydride 1 in the presence of quinine. As in the case of quinidine, the transition states of addition of methanol from both left and right sides of 1 have been located with the Open(3) conformation of quinine (Figure 3.12). In this way, both reaction pathways whose products are 2 and *ent*-2 and their barriers have been considered and compared with experimental findings which have shown that the quinine catalyzed reaction prefers to yield *ent*-2 [68]. Similar to quinidine transition structures, when addition of methanol takes place from the left side (TS-QN-left), the hydroxyl group of quinine makes a hydrogen bond with the right carbonyl oxygen with 1.87 Å distance, and for the attack of methanol to right carbonyl carbon (TS-QN-left), the hydrogen bond forms between the hydroxyl group of quinine and the left carbonyl oxygen with 1.88 Å distance. Like quinidine, quinine assists in the stabilization of the system and the proton transfer between methanol and the anhydride oxygen. In both transition structures, the critical distance between the carbonyl carbon and the anhydride oxygen is around 1.5 Å. It has been found that the left attack of methanol to the anhydride 1 with quinine can occur through another structure (TS-QN-left2) in which hydrogen bond forms between the hydroxyl group of quinine and the anhydride oxygen with 1.98 Å distance (Figure 3.12). Due to the structure of quinine, such additional transition state has not been found for the right attack of methanol.

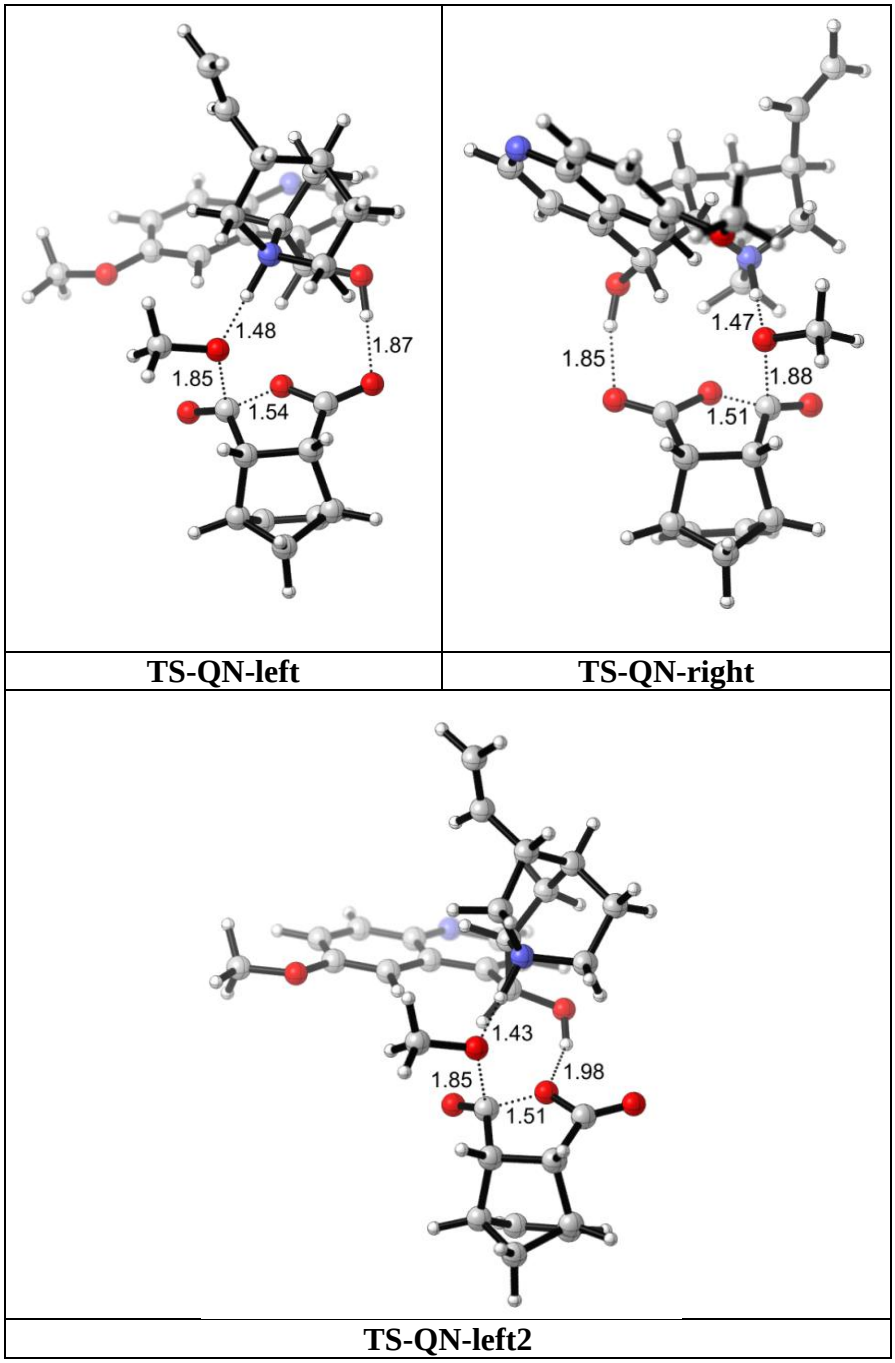

TS-QN-left	TS-QN-right
TS-QN-left2	

Figure 3.12. Quinine catalyzed transition state structures.

IRC calculations have verified that TS-QN-left and TS-QN-left2 gives the product 2, meanwhile TS-QN-right connects to product *ent*-2. The most stable reactant for quinine catalyzed system has been chosen from the obtained 3 reactants and activation barriers have been calculated (Table 3.5). The characteristic dihedral angles of quinine in the transition state structures have also been displayed in Table 3.5 to show their similarity

with the angles of the previously located Open(3) conformation of quinine (τ_1: 99.2, τ_2:157.7, and τ_3:285.6).

Table 3.5. Gibbs free energy barriers ($\Delta G^{\ddagger}$) of asymmetric desymmetrization of *meso* anhydride 1 with quinine and characteristic dihedral angles of quinine.

TS	**Product**	**Quinine**			**$\Delta G^{\ddagger}$ (kcal/mol)**	
		τ_1	**τ_2**	**τ_3**	**B3LYP/6-31+G(d,p)**	**M06-2X/6-31+G(d,p)[a]**
TS-QN-left	**2**	106.0	166.4	294.0	25.2	21.9
TS-QN-left2	**2**	104.8	171.0	299.2	24.1	18.8
TS-QN-right	***ent*-2**	103.4	161.4	291.0	21.7	16.4

[a]The values are obtained from single point calculations on the B3LYP/6-31+G(d,p) optimized geometries

The activation barrier of the reaction whose product is *ent*-2 is 2.4 kcal/mol lower than the other reactions that yield product *ent*-2 according to both methods as expected from experimental findings [68] (Table 3.5). When methanol attack takes place from the left hand side, the hydroxyl group of quinine prefers to make a hydrogen bond with the anhydride oxygen. Hence, this time, TS-QN-left2 and TS-QN-right have been taken into account to compare the energy barrier difference between the reaction of 2 with *ent*-2. Upon checking the charges of the methanol oxygen and the carbonyl carbon to be attacked, charges are found to be distributed better in TS-QN-right (C:-0.865 and O: -0.439) than TS-QN-left2 (C:-1.199 and O: -0.362) which explains the energy difference between these transition structures. The difference between M06-2X and B3LYP results are similar with the ones obtained for quinidine; the M06 results are slightly lower. To sum up, it has been found that the quinine catalyzed reaction yielding *ent*-2 is energetically preferred and this result is consistent with experimentally determined enantioselectivity [68].

After modeling the transition states and finding the best transition structures for both quinine (TS-QN-left2 and TS-QN-right) and quinidine (TS-QD-left and TS-QD-right2) and best reactants, the effect of solvent to the activation barriers has been investigated. Although the experiments were performed in a toluene/CCl_4 mixture and 99% enantiomeric excess of both products were obtained, Bolm *et al.* have emphasized that the use of toxic CCl_4 can be avoided, since the reactions have also been carried out in pure toluene and almost the same enantioselectivities have been obtained [68]. Thus, toluene

has been considered as solvent in calculations of the solvent effect. The obtained results are summarized in Table 3.6.

Table 3.6. Gibbs free energy barriers ($\Delta G^{\neq}$) of asymmetric desymmetrization of *meso* anhydride 1 with quinine and quinidine in toluene.[a]

TS	**Product**	$\Delta G^{\neq}_{toluene}$ **(kcal/mol)**	
		B3LYP/6-31+G(d,p)	**M06-2X/6-31+G(d,p)**
TS-QD-left	**2**	20.2	16.0
TS-QD-right2	***ent*-2**	22.0	18.1
TS-QN-left2	**2**	22.6	17.4
TS-QN-right	***ent*-2**	20.8	15.4

[a]Values are obtained from single point PCM calculations on the B3LYP/6-31+G(d,p) optimized geometries.

The obtained barriers of the reactions are slightly lower than the gas phase results. The energy difference between the barriers of the reactions of 2 and *ent*-2 also decreases for both quinine and quinidine; however they are in accordance with the experimental results. In order to perform comparison of calculated results with experimental findings accurately, the enantiomeric excess percent of the products in the presence of quinine and quinidine have been calculated by using Boltzmann distribution equation which is:

$$\frac{n_2}{n_{ent-2}} = e^{-\frac{\Delta(\Delta G^{\neq})}{RT}} \qquad (5.1)$$

where $\Delta(\Delta G^{\neq})$ is the energy difference between 2 and *ent*-2, R is the gas constant and T is the temperature which is 298.15 K in this case. The experimental and calculated enantiomeric excess percentages are given in Table 3.7. It has been found that, the experimental and calculated results are in accordance with each other and they follow the same trend.

In this part of study, the concerted mechanism of the asymmetric desymmetrization of *meso* anhydride 1 in presence of both quinine and quinidine has been explored seperately. It has been shown that, quinidine catalyzed methanolysis of 1 has lower energy barrier when the product is 2 and when it is *ent*-2, quinine catalyzed reaction has been preferred energetically. In summary, the preferred reaction pathways which are the

reaction through TS-QD-left to give product 2 for quinidine and the reaction through TS-QN-right to give product *ent*-2 for quinine are shown in Figure 3.13 and Figure 3.14.

Table 3.7. The experimental and calculated enantiomeric excess percentages of the products in toluene.

ee (%) of product	Quinine		Quinidine	
	Experimental	**Calculated**	**Experimental**	**Calculated**
2	1[a]	3	96[b]	97
***ent*-2**	99[a]	97	4[b]	3

[a]Solvent: Toluene/CCl_4 mixture; [b]Solvent: Toluene

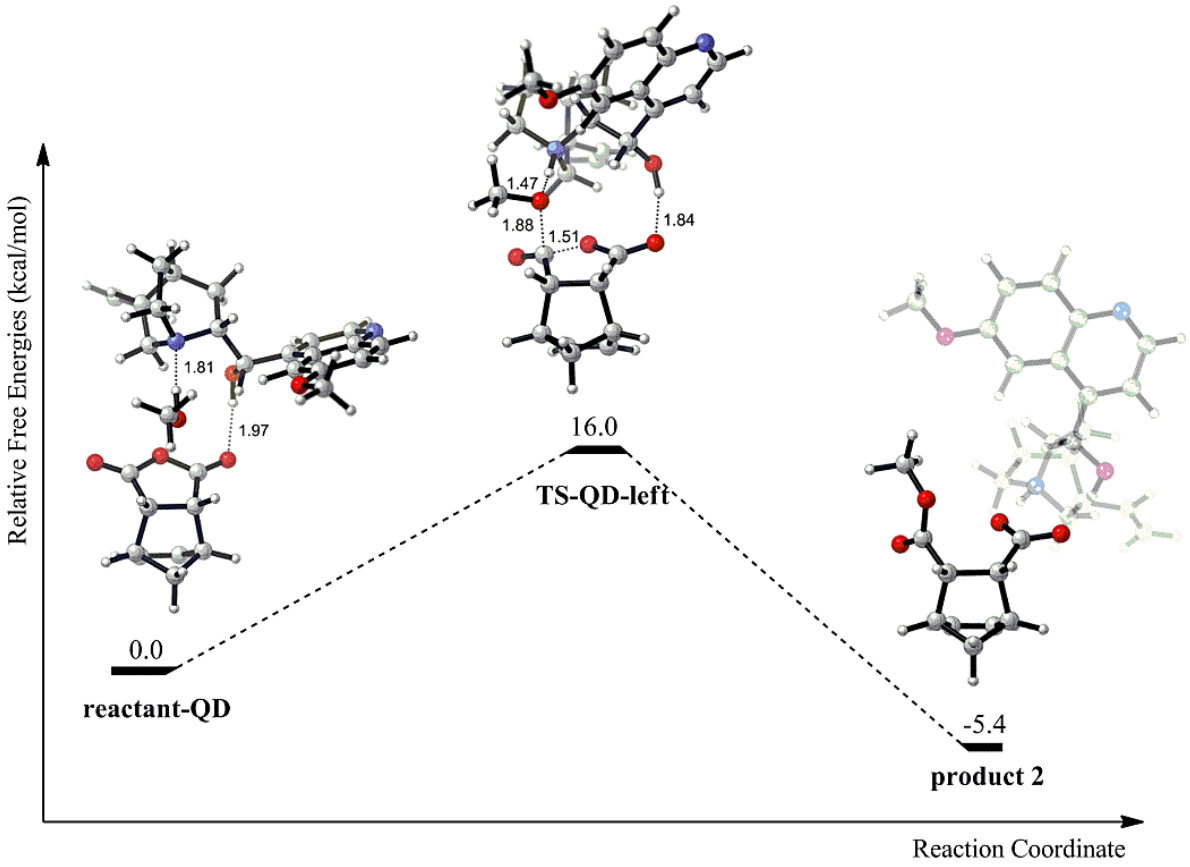

Figure 3.13. Potential energy surface for asymmetric desymmetrization of cyclic *meso* anhydride 1 with quinidine (Energies correspond to PCM calculations with M06-2X/6-31+G(d,p)//B3LYP/6-31+G(d,p)).

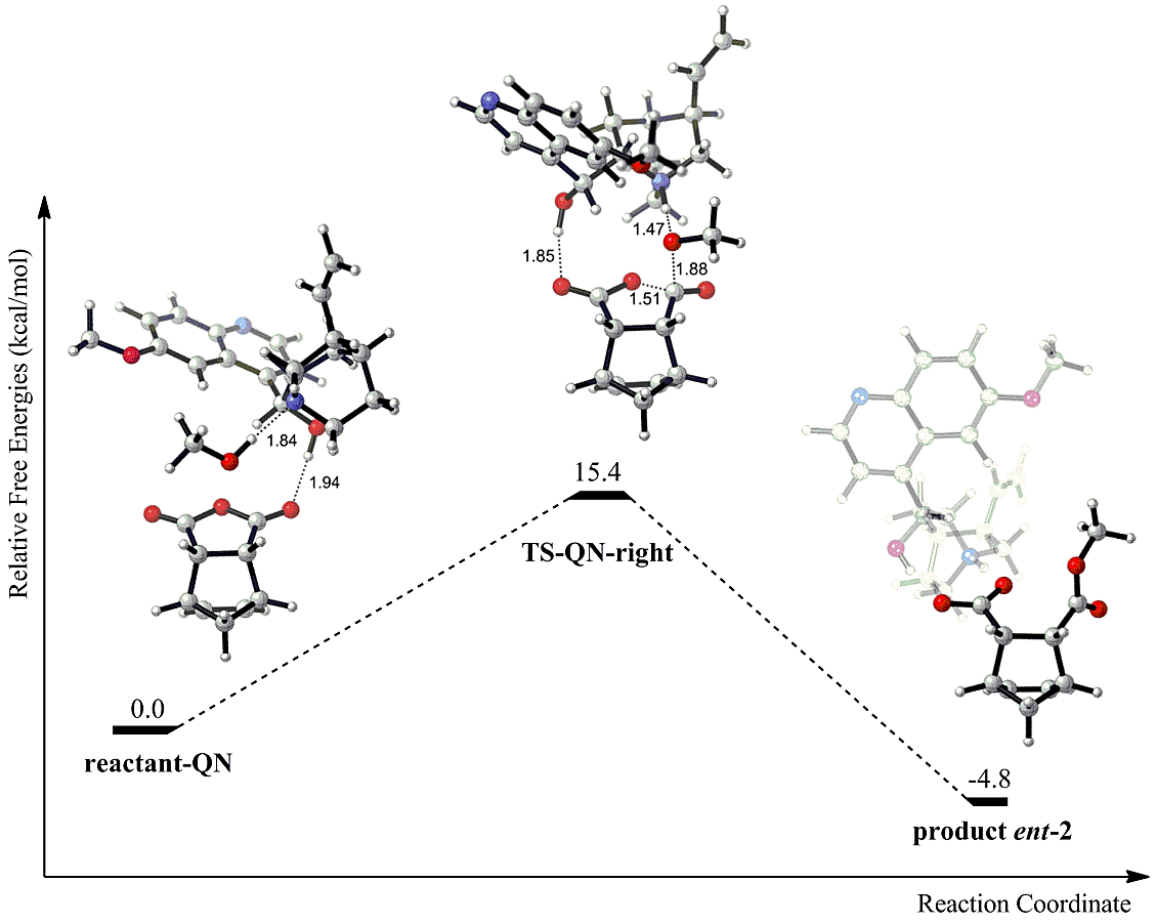

Figure 3.14. Potential energy surface for asymmetric desymmetrization of cyclic *meso* anhydride 1 with quinine (Energies correspond to PCM calculations with M06-2X/6-31+G(d,p)//B3LYP/6-31+G(d,p)).

3.3.2.2. Stepwise Mechanism. In the stepwise mechanism, the addition of methanol to *meso* anhydride in the presence of cinchona alkaloids and opening of the ring that yields the hemi-ester product takes place in steps. Instead of the hemi-ester product formation, a tetrahedral intermediate is formed in the first step. Then this intermediate gives the final product after ring opening step (Figure 3.15)

Recent studies have shown that the rate determining step of stepwise mechanism of the methanolysis of cyclic *meso* anhydrides is the first step which is addition of methanol that connects to intermediate [67]. For this reason, only activation barrier of addition of methanol has been calculated by modeling first step in order to compare it with the concerted activation barriers. Since it has been proved in the previous section that left

addition of methanol to cyclic *meso* anhydride 1 is preferred in the presence of quinidine through TS-QD-left, and right addition takes place with quinine through TS-QN-right, their stepwise transition state structures have been located as a first step in this section. The intermediate products and reactants have been verified with IRC calculations and all of these structures are given in the potential energy surface diagrams (Figure 3.16 and Figure 3.17). The located transition states differ from the concerted transition structures in two points which are the critical distance which is shorter in stepwise case (1.45 Å) and the location of the hydrogen bond that has a stabilizing role. In stepwise transition states, the hydroxyl group of the cinchona alkaloid makes a hydrogen bond with the carbonyl oxygen at the side of methanol attack. To be more precise, in S-TS-QD-left, hydroxyl group makes a hydrogen bond with the left carbonyl oxygen with 1.89 Å distance and in S-TS-QN-right, this hydrogen bond takes place at right side with 1.84 Å distance.

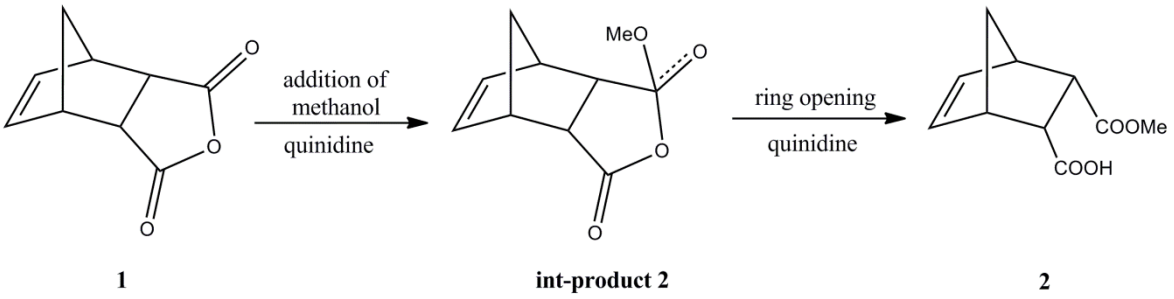

Figure 3.15. Stepwise mechanism of methanolysis of *meso* anhydride 1 with quinidine.

All activation barriers with both methods are summarized in Table 3.8. For comparison purposes, the corresponding concerted barriers are also given in brackets. The obtained activation barriers for the first step of the stepwise mechanism are higher than the concerted barriers which prove that the asymmetric desymmetrization of cyclic *meso* anhydride 1 prefers to take place in concerted pathway.

Table 3.8. Gibbs free energy barriers ($\Delta G^{\ddagger}$) of stepwise mechanism with quinine and quinidine.

TS	**Product**	**$\Delta G^{\ddagger}$ (kcal/mol)**	
		B3LYP/6-31+G(d,p)	**M06-2X/6-31+G(d,p)[a]**
S-TS-QD-left	**2**	22.8 [21.3][b]	17.9 [17.1][b]
S-TS-QN-right	***ent*-2**	23.0 [21.7][b]	17.0 [16.4][b]

[a]The values are obtained from single point calculations on the B3LYP/6-31+G(d,p) optimized geometries. [b]Values in brackets are corresponding concerted barriers.

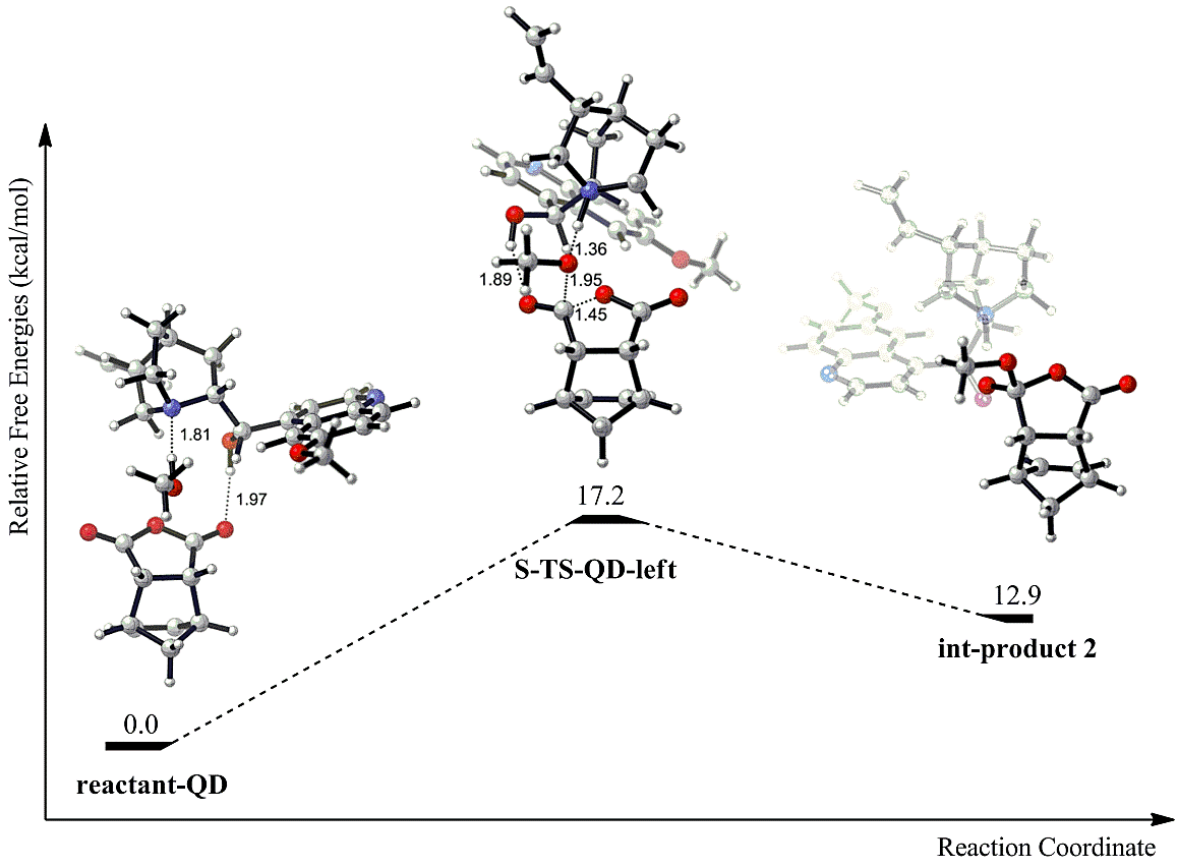

Figure 3.16. Potential energy surface for stepwise mechanism with quinidine (Energies correspond to PCM calculations with M06-2X/6-31+G(d,p)//B3LYP/6-31+G(d,p)).

Nevertheless, the solvent effect to the mechanism has also been taken into account in order to check results against the concerted barriers which include solvent effect. The results which are shown in Table 3.9 show that barriers of concerted pathway are lower than the stepwise barriers in case of solvent effect, too.

Table 3.9. Gibbs free energy barriers ($\Delta G^{\ddagger}$) of stepwise mechanism with quinine and quinidine in toluene.

TS	Product	$\Delta G^{\ddagger}_{toluene}$ (kcal/mol)	
		B3LYP/6-31+G(d,p)	M06-2X/6-31+G(d,p)[a]
S-TS-QD-left	**2**	22.2 [20.2][b]	17.2 [16.0][b]
S-TS-QN-right	***ent*-2**	22.4 [20.8][b]	16.4 [15.4][b]

[a]The values are obtained from single point calculations on the B3LYP/6-31+G(d,p) optimized geometries [b]Values in brackets are corresponding concerted barriers.

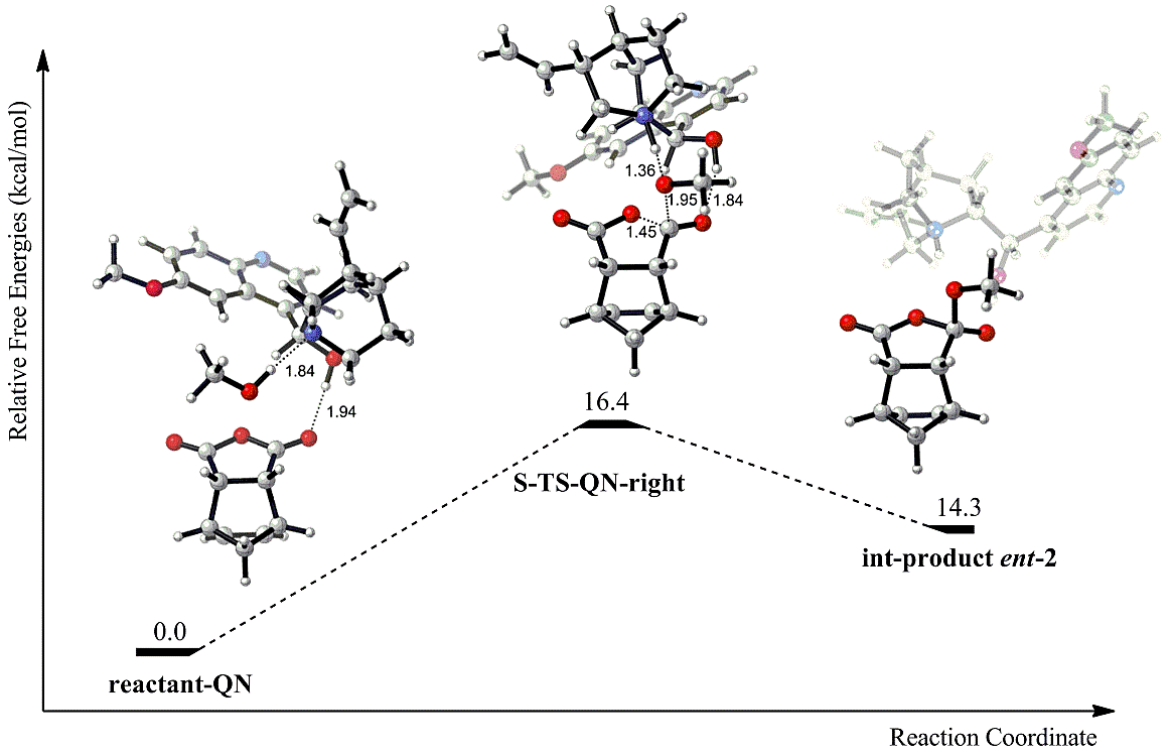

Figure 3.17. Potential energy surface for stepwise mechanism with quinine (Energies correspond to PCM calculations with M06-2X/6-31+G(d,p)//B3LYP/6-31+G(d,p)).

When all results obtained from stepwise mechanism are compared with concerted mechanism results, it is seen that the concerted pathway is energetically favored over the stepwise pathway since its barriers are higher than the concerted barriers in both gas phase and solvent.

3.4. Conclusions and Future Work

In this study, the asymmetric desymmetrization of cyclic *meso* anhydrides in the presence of cinchona alkaloids (quinine and quinidine) has been subjected to a computational analysis. The conformational analysis of quinine and quinidine pseudoenantiomeric pairs has been carried out. Then, the concerted and stepwise pathways have been explored for the addition of methanol to the anhydride in the presence of the cinchona catalyst.

Among all the previously proposed and currently studied geometries of cinchona alkaloids, Open(3) conformation has been found to be the most stable structure for both quinine and quinidine. Therefore, this conformation has been used during modeling the mechanisms.

The stepwise mechanism is shown to be energetically less plausible than the concerted mechanism. By this fact it can be proposed that, the addition of methanol to the *meso* anhydrides and the ring-opening of the anhydride occurs in a single step in the presence of quinine and quinidine. The obtained activation barriers of concerted mechanism and calculated enantiomeric excess percentages of the products in the presence of both catalysts reveal that quinidine catalyzed reaction yields product 2 since the barrier increases when it yields product *ent*-2, and when the catalyst is changed to quinine, the reaction whose product is *ent*-2 is energetically favored as experimentally proposed [68]. The importance of the cinchona alkaloids in this reaction can be correlated with their stabilizing role in transition state structures and assistance to proton transfer between methanol and anhydride.

As a future work, the quinine and quinidine catalyzed stepwise mechanisms will also be investigated for the attacks which are found to be unfavorable in the concerted pathways (TS-QD-right and TS-QD-left). All located structures; transition states, reactants and products will also be optimized with M06-2X/6-31+G(d,p) method to obtain more accurate geometries in terms of non-covalent interactions. All geometries will be also subjected to PCM optimizations for better understanding of the solvent effect to reaction pathway. In addition, the reactions will be modeled with the other obtained most stable conformations of the cinchona catalysts which are Closed(1) and Closed(2) in order to explore the importance of the conformation of the catalyst.

REFERENCES

1. Lambert, J. B., G. T. Wang, D. E. Huseland and L. C. Takiff, "Acid-Catalyzed Ring Chain Tautomerism in 1,3-Diazolidines", *Journal of Organic Chemistry,* Vol. 52, No. 1, pp. 68-71, 1987.

2. Keiko, N. A., N. V. Vchislo, L. G. Stepanova, L. I. Larina, Y. A. Chuvashev and E. A. Funtikova, "Condensation of 2-Alkoxypropenals with N,N- and N,O-1,2-Binucleophiles. A Route to 2-(1'-Alkoxyvinyl)Imidazo-Lidines and -Oxazolidines", *Chemistry of Heterocyclic Compounds,* Vol. 44, No. 12, pp. 1466-1471, 2008.

3. Szatmari, I., T. A. Martinek, L. Lazar, A. Koch, E. Kleinpeter, K. Neuvonen and F. Fulop, "Stereoelectronic Effects in Ring-Chain Tautomerism of 1,3-Diarylnaphth 1,2-E 1,3 Oxazines and 3-Alkyl-1-Arylnaphth 1,2-E 1,3 Oxazines", *Journal of Organic Chemistry,* Vol. 69, No. 11, pp. 3645-3653, 2004.

4. Shi, S. L., L. W. Xu, K. Oisaki, M. Kanai and M. Shibasaki, "Identification of Modular Chiral Bisphosphines Effective for Cu(I)-Catalyzed Asymmetric Allylation and Propargylation of Ketones", *Journal of the American Chemical Society,* Vol. 132, No. 19, pp. 6638-6639, 2010.

5. Shintani, Y., T. Tanaka and Y. Nozaki, "Gs-164, a Small Synthetic Compound, Stimulates Tubulin Polymerization by a Similar Mechanism to That of Taxol", *Cancer Chemotherapy and Pharmacology,* Vol. 40, No. 6, pp. 513-520, 1997.

6. Desino, K. E., S. Ansar, G. I. Georg, R. H. Himes, M. L. Michaelis, D. R. Powell, E. A. Reiff, H. Telikepalli and K. L. Audus, "(3r,5s,7as)-(3,5-Bis(4-Fluorophenyl)Tetrahydro-1h-Oxazolo 3,4-C Oxazol-7 a-Yl)Methanol, a Novel Neuroprotective Agent", *Journal of Medicinal Chemistry,* Vol. 52, No. 23, pp. 7537-7543, 2009.

7. Saiz, C., P. Wipf and G. Mahlerf, "Synthesis and Ring-Chain-Ring Tautomerism of Bisoxazolidines, Thiazolidinyloxazolidines, and Spirothiazolidines", *Journal of Organic Chemistry,* Vol. 76, No. 14, pp. 5738-5746, 2011.

8. Korotaev, V. Y., A. Y. Barkov, P. A. Slepukhin, M. I. Kodess and V. Y. Sosnovskikh, "Unusual Ring-Chain Tautomerism in Bicyclo 4.2.0 Octane Derivatives", *Tetrahedron Letters,* Vol. 52, No. 23, pp. 3029-3032, 2011.

9. Delaine, T., V. Bernardes-Genisson, J. L. Stigliani, H. Gornitzka, B. Meunier and J. Bernadou, "Ring-Chain Tautomerism of Simplified Analogues of Isoniazid-Nad(P) Adducts: An Experimental and Theoretical Study", *European Journal of Organic Chemistry,* Vol. No. 10, pp. 1624-1630, 2007.

10. Perez, S., C. Lopez, A. Caubet, A. Roig and E. Molins, "Ring-Chain Tautomerism of the Novel 2-Ferrocenyl-2,4-Dihydro-1h-3,1-Benzoxazine", *Journal of Organic Chemistry,* Vol. 70, No. 12, pp. 4857-4860, 2005.

11. Demir-Ordu, O. and I. Dogan, "Axially Chiral N-(O-Aryl)-4-Hydroxy-2-Oxazolidinone Derivatives from Diastereoselective Reduction of N-(O-Aryl)-2,4-Oxazolidinediones: Thermally Interconvertible Atropisomers Via Ring-Chain-Ring Tautomerization", *Chirality,* Vol. 22, No. 7, pp. 641-654, 2010.

12. Sinkkonen, J., V. Ovcharenko, K. N. Zelenin, I. P. Bezhan, B. A. Chakchir, F. Al-Assar and K. Pihlaja, "Stereoisomerism and Ring-Chain Tautomerism in 1-Hydroxy-2,3-Dihydro-1h-Pyrazolo 1,2-a Pyridazine-5,8-Diones and 1-Hydroxy- and 1-Amino-2,3-Dihydro-1h-Pyrazolo 1,2-B Phthalazine-5,10-Diones", *European Journal of Organic Chemistry,* Vol. No. 20, pp. 3447-3454, 2002.

13. Jin, J. A., A. Morales-Ramos, P. Eidam, J. Mecom, Y. Li, C. Brooks, M. Hilfiker, D. Zhang, N. Wang, D. C. Shi, P. S. Tseng, K. Wheless, B. Budzik, K. Evans, J. P. Jaworski, J. Jugus, L. Leon, C. Wu, M. Pullen, B. Karamshi, P. Rao, E. Ward, N. Laping, C. Evans, C. Leach, D. Holt, X. Su, D. Morrow, H. Fries, K. Thorneloe and R. Edwards, "Novel 3-Oxazolidinedione-6-Aryl-

Pyridinones as Potent, Selective, and Orally Active Ep3 Receptor Antagonists", *Acs Medicinal Chemistry Letters,* Vol. 1, No. 7, pp. 316-320, 2010.

14. Lohray, B. B. and V. Bhushan, "Advances in Insulin Sensitizers", *Current Medicinal Chemistry,* Vol. 11, No. 18, pp. 2467-2503, 2004.

15. Momose, Y., T. Maekawa, T. Yamano, M. Kawada, H. Odaka, H. Ikeda and T. Sohda, "Novel 5-Substituted 2,4-Thiazolidinedione and 2,4-Oxazolidinedione Derivatives as Insulin Sensitizers with Antidiabetic Activities", *Journal of Medicinal Chemistry,* Vol. 45, No. 7, pp. 1518-1534, 2002.

16. Aitken, R. A. and S. N. Kilenyi, *Asymmetric Synthesis*, Blackie Academic Professional, London, 1992.

17. Lin, G. K. and Y. M. Li, *Principles and Applications of Asymmetric Synthesis*, Wiley Interscience Publication, New York, 2001.

18. Berkessel, A. and H. Gröger, *Asymmetric Organocatalysis,* Wiley-VCH, Weinheim, 2005.

19. Ward, R. S., "Nonenzymatic Asymmetric Transformations Involving Symmetrical Bifunctional Compounds", *Chemical Society Reviews,* Vol. 19, No. 1, pp. 1-19, 1990.

20. Willis, M. C., "Enantioselective Desymmetrisation", *Journal of the Chemical Society-Perkin Transactions 1,* Vol. No. 13, pp. 1765-1784, 1999.

21. Chen, Y. G., P. McDaid and L. Deng, "Asymmetric Alcoholysis of Cyclic Anhydrides", *Chemical Reviews,* Vol. 103, No. 8, pp. 2965-2983, 2003.

22. Spivey, A. C. and B. I. Andrews, "Catalysis of the Asymmetric Desymmetrization of Cyclic Anhydrides by Nucleophilic Ring-Opening with Alcohols", *Angewandte Chemie-International Edition,* Vol. 40, No. 17, pp. 3131-3134, 2001.

23. Wong, C. H. and G. M. Whitesides, *Enzymes in Synthetic Organic Chemistry*, Elsevier, Oxford, 1994.

24. Atodiresei, L., I. Schiffers and C. Bolm, "Stereoselective Anhydride Openings", *Chemical Reviews*, Vol. 107, No. 12, pp. 5683-5712, 2007.

25. Aydeniz, Y., F. Oguz, A. Yaman, A. S. Konuklar, I. Dogan, V. Aviyente and R. A. Klein, "Barriers to Internal Rotation around the C-N Bond in 3-(O-Aryl)-5-Methyl-Rhodanines Using Nmr Spectroscopy and Computational Studies. Electron Density Topological Analysis of the Transition States", *Organic & Biomolecular Chemistry*, Vol. 2, No. 17, pp. 2426-2436, 2004.

26. Demir-Ordu, O., E. M. Yilmaz and I. Dogan, "Determination of the Absolute Stereochemistry and the Activation Barriers of Thermally Interconvertible Heterocyclic Compounds Bearing a Naphthyl Substituent", *Tetrahedron-Asymmetry*, Vol. 16, No. 22, pp. 3752-3761, 2005.

27. Ordu, O. D. and K. Dogan, "Determination of Energy Barriers to Rotation and Absolute Conformations of Thermally Interconvertible 5,5-Dimethyl-3(O-Aryl)-2,4-Oxazolidinedione Enantiomers", *Tetrahedron-Asymmetry*, Vol. 15, No. 6, pp. 925-933, 2004.

28. Yilmaz, E. M. and I. Dogan, "Axially Chiral N-(O-Aryl)-2-Thioxo-Oxazolidine-4-One and Rhodanine Derivatives: Enantiomeric Separation and Determination of Racemization Barriers", *Tetrahedron-Asymmetry*, Vol. 19, No. 18, pp. 2184-2191, 2008.

29. Clayden, J., W. J. Moran, P. J. Edwards and S. R. LaPlante, "The Challenge of Atropisomerism in Drug Discovery", *Angewandte Chemie-International Edition*, Vol. 48, No. 35, pp. 6398-6401, 2009.

30. Guo, F. H., L. C. Konkol and R. J. Thomson, "Enantioselective Synthesis of Biphenols from 1,4-Diketones by Traceless Central-to-Axial Chirality Exchange", *Journal of the American Chemical Society,* Vol. 133, No. 1, pp. 18-20, 2011.

31. Gustafson, J. L., D. Lim and S. J. Miller, "Dynamic Kinetic Resolution of Biaryl Atropisomers Via Peptide-Catalyzed Asymmetric Bromination", *Science,* Vol. 328, No. 5983, pp. 1251-1255, 2010.

32. Cozzi, P. G., E. Emer and A. Gualandi, "Atroposelective Organocatalysis", *Angewandte Chemie-International Edition,* Vol. 50, No. 17, pp. 3847-3849, 2011.

33. Paul, B., G. L. Butterfoss, M. G. Boswell, P. D. Renfrew, F. G. Yeung, N. H. Shah, C. Wolf, R. Bonneau and K. Kirshenbaum, "Peptoid Atropisomers", *Journal of the American Chemical Society,* Vol. 133, No. 28, pp. 10910-10919, 2011.

34. Roussel, C., M. Adjimi, A. Chemlal and A. Djafri, "Comparison of Racemization Processes in 1-Arylpyrimidine-2-Thione and 3-Arylthiazoline-2-Thione Atropisomers and Their Oxygen Analogs", *Journal of Organic Chemistry,* Vol. 53, No. 21, pp. 5076-5080, 1988.

35. Becke, A. D., "Density-Functional Thermochemistry .3. The Role of Exact Exchange", *Journal of Chemical Physics,* Vol. 98, No. 7, pp. 5648-5652, 1993.

36. Gaussian 03, Revision C.02, Frisch, M. J., Gaussian, Inc., Wallingford CT, 2004.

37. Gaussian 09, Revision A.1, Frisch, M. J., Gaussian, Inc., Wallingford CT, 2009.

38. Fukui, K., "The Path of Chemical-Reactions - the Irc Approach", *Accounts of Chemical Research,* Vol. 14, No. 12, pp. 363-368, 1981.

39. Tomasi, J., B. Mennucci and R. Cammi, "Quantum Mechanical Continuum Solvation Models", *Chemical Reviews,* Vol. 105, No. 8, pp. 2999-3093, 2005.

40. Barone, V. and M. Cossi, "Quantum Calculation of Molecular Energies and Energy Gradients in Solution by a Conductor Solvent Model", *Journal of Physical Chemistry A*, Vol. 102, No. 11, pp. 1995-2001, 1998.

41. Rappe, A. K., C. J. Casewit, K. S. Colwell, W. A. Goddard and W. M. Skiff, "Uff, a Full Periodic-Table Force-Field for Molecular Mechanics and Molecular-Dynamics Simulations", *Journal of the American Chemical Society*, Vol. 114, No. 25, pp. 10024-10035, 1992.

42. Boese, A. D. and J. M. L. Martin, "Development of Density Functionals for Thermochemical Kinetics", *Journal of Chemical Physics*, Vol. 121, No. 8, pp. 3405-3416, 2004.

43. Zhao, Y. and D. G. Truhlar, "Hybrid Meta Density Functional Theory Methods for Thermochemistry, Thermochemical Kinetics, and Noncovalent Interactions: The Mpw1b95 and Mpwb1k Models and Comparative Assessments for Hydrogen Bonding and Van Der Waals Interactions", *Journal of Physical Chemistry A*, Vol. 108, No. 33, pp. 6908-6918, 2004.

44. Headgordon, M., J. A. Pople and M. J. Frisch, "Mp2 Energy Evaluation by Direct Methods", *Chemical Physics Letters*, Vol. 153, No. 6, pp. 503-506, 1988.

45. Gerenkamp, M. and S. Grimme, "Spin-Component Scaled Second-Order Moller-Plesset Perturbation Theory for the Calculation of Molecular Geometries and Harmonic Vibrational Frequencies", *Chemical Physics Letters*, Vol. 392, No. 1-3, pp. 229-235, 2004.

46. Zhao, Y. and D. G. Truhlar, "The M06 Suite of Density Functionals for Main Group Thermochemistry, Thermochemical Kinetics, Noncovalent Interactions, Excited States, and Transition Elements: Two New Functionals and Systematic Testing of Four M06-Class Functionals and 12 Other Functionals", *Theoretical Chemistry Accounts*, Vol. 120, No. 1-3, pp. 215-241, 2008.

47. Zhao, Y. and D. G. Truhlar, "Density Functionals with Broad Applicability in Chemistry", *Accounts of Chemical Research,* Vol. 41, No. 2, pp. 157-167, 2008.

48. Seyden-Penne, J., *Reductions by the Alumino- and Borohydrides in Organic Synthesis*, Wiley-VCH, 1997.

49. Catak, S., M. D'Hooghe, N. De Kimpe, M. Waroquier and V. Van Speybroeck, "Intramolecular Pi-Pi Stacking Interactions in 2-Substituted N,N-Dibenzylaziridinium Ions and Their Regioselectivity in Nucleophilic Ring-Opening Reactions", *Journal of Organic Chemistry,* Vol. 75, No. 3, pp. 885-896, 2010.

50. Catak, S., G. Monard, V. Aviyente and M. F. Ruiz-Lopez, "Reaction Mechanism of Deamidation of Asparaginyl Residues in Peptides: Effect of Solvent Molecules", *Journal of Physical Chemistry A,* Vol. 110, No. 27, pp. 8354-8365, 2006.

51. Catak, S., G. Monard, V. Aviyente and M. F. Ruiz-Lopez, "Computational Study on Nonenzymatic Peptide Bond Cleavage at Asparagine and Aspartic Acid", *Journal of Physical Chemistry A,* Vol. 112, No. 37, pp. 8752-8761, 2008.

52. Catak, S., G. Monard, V. Aviyente and M. F. Ruiz-Lopez, "Deamidation of Asparagine Residues: Direct Hydrolysis Versus Succinimide-Mediated Deamidation Mechanisms", *Journal of Physical Chemistry A,* Vol. 113, No. 6, pp. 1111-1120, 2009.

53. Durak, A. T., H. Gokcan and F. A. S. Konuklar, "Theoretical Studies on the Inactivation Mechanism of Gamma-Aminobutyric Acid Aminotransferase", *Organic & Biomolecular Chemistry,* Vol. 9, No. 14, pp. 5162-5171, 2011.

54. Agmon, N., "The Grotthuss Mechanism", *Chemical Physics Letters,* Vol. 244, No. 5-6, pp. 456-462, 1995.

55. Liu, L. P., D. Malhotra, R. S. Paton, K. N. Houk and G. B. Hammond, "The 4+2 , Not 2+2 , Mechanism Occurs in the Gold-Catalyzed Intramolecular Oxygen

Transfer Reaction of 2-Alkynyl-1,5-Diketones", *Angewandte Chemie-International Edition*, Vol. 49, No. 48, pp. 9132-9135, 2010.

56. France, S., D. J. Guerin, S. J. Miller and T. Lectka, "Nucleophilic Chiral Amines as Catalysts in Asymmetric Synthesis", *Chemical Reviews*, Vol. 103, No. 8, pp. 2985-3012, 2003.

57. Johansson, C. C. C., N. Bremeyer, S. V. Ley, D. R. Owen, S. C. Smith and M. J. Gaunt, "Enantioselective Catalytic Intramolecular Cyclopropanation Using Modified Cinchona Alkaloid Organocatalysts", *Angewandte Chemie-International Edition*, Vol. 45, No. 36, pp. 6024-6028, 2006.

58. Kolb, H. C., M. S. Vannieuwenhze and K. B. Sharpless, "Catalytic Asymmetric Dihydroxylation", *Chemical Reviews*, Vol. 94, No. 8, pp. 2483-2547, 1994.

59. Burgi, T. and A. Baiker, "Conformational Behavior of Cinchonidine in Different Solvents: A Combined Nmr and Ab Initio Investigation", *Journal of the American Chemical Society*, Vol. 120, No. 49, pp. 12920-12926, 1998.

60. Dijkstra, G. D. H., R. M. Kellogg and H. Wynberg, "Conformational Study of Cinchona Alkaloids - a Combined Nmr and Molecular-Orbital Approach", *Journal of Organic Chemistry*, Vol. 55, No. 25, pp. 6121-6131, 1990.

61. Dijkstra, G. D. H., R. M. Kellogg, H. Wynberg, J. S. Svendsen, I. Marko and K. B. Sharpless, "Conformational Study of Cinchona Alkaloids - a Combined Nmr, Molecular Mechanics, and X-Ray Approach", *Journal of the American Chemical Society*, Vol. 111, No. 21, pp. 8069-8076, 1989.

62. Meier, D. M., A. Urakawa, N. Turra, H. Ruegger and A. Baiker, "Hydrogen-Bonding Interactions in Cinchonidine-2-Methyl-2-Hexenoic Acid Complexes: A Combined Spectroscopic and Theoretical Study", *Journal of Physical Chemistry A*, Vol. 112, No. 27, pp. 6150-6158, 2008.

63. Urakawa, A., D. M. Meier, H. Rugger and A. Baiker, "Conformational Behavior of Cinchonidine Revisited: A Combined Theoretical and Experimental Study", *Journal of Physical Chemistry A*, Vol. 112, No. 31, pp. 7250-7255, 2008.

64. Hiratake, J., Y. Yamamoto and J. Oda, "Catalytic Asymmetric Induction from Prochiral Cyclic Acid Anhydrides Using Cinchona Alkaloids", *Journal of the Chemical Society-Chemical Communications*, Vol. No. 23, pp. 1717-1719, 1985.

65. Aitken, R. A., J. Gopal and J. A. Hirst, "Catalytic Asymmetric-Synthesis of Highly Functionalized Compounds with 6 Contiguous Stereocenters", *Journal of the Chemical Society-Chemical Communications*, Vol. No. 10, pp. 632-634, 1988.

66. Bolm, C., A. Gerlach and C. L. Dinter, "Simple and Highly Enantioselective Nonenzymatic Ring Opening of Cyclic Prochiral Anhydrides", *Synlett*, Vol. No. 2, pp. 195-196, 1999.

67. Dedeoglu, B., S. Catak, K. N. Houk and V. Aviyente, "A Theoretical Study of the Mechanism of the Desymmetrization of Cyclic Meso-Anhydrides by Chiral Amino Alcohols", *Chemcatchem*, Vol. 2, No. 9, pp. 1122-1129, 2010.

68. Bolm, C., I. Schiffers, C. L. Dinter and A. Gerlach, "Practical and Highly Enantioselective Ring Opening of Cyclic Meso-Anhydrides Mediated by Cinchona Alkaloids", *Journal of Organic Chemistry*, Vol. 65, No. 21, pp. 6984-6991, 2000.

69. Parr, R. G. and W. Yang, *Density Functional Theory of Atoms and Molecules*, Oxford University Press, New York, 1989.

70. Tomasi, J., B. Mennucci and E. Cances, "The Ief Version of the Pcm Solvation Method: An Overview of a New Method Addressed to Study Molecular Solutes at the Qm Ab Initio Level", *Journal of Molecular Structure-Theochem*, Vol. 464, No. 1-3, pp. 211-226, 1999.